



HAL
open science

Computational and robotic modeling reveal parsimonious combinations of interactions between individuals in schooling fish

Liu Lei, Ramón Escobedo, Clément Sire, Guy Théraulaz

► **To cite this version:**

Liu Lei, Ramón Escobedo, Clément Sire, Guy Théraulaz. Computational and robotic modeling reveal parsimonious combinations of interactions between individuals in schooling fish. *PLoS Computational Biology*, 2020, 16 (3), pp.e1007194. 10.1371/journal.pcbi.1007194 . hal-03363016v2

HAL Id: hal-03363016

<https://hal.science/hal-03363016v2>

Submitted on 2 Oct 2021

HAL is a multi-disciplinary open access archive for the deposit and dissemination of scientific research documents, whether they are published or not. The documents may come from teaching and research institutions in France or abroad, or from public or private research centers.

L'archive ouverte pluridisciplinaire **HAL**, est destinée au dépôt et à la diffusion de documents scientifiques de niveau recherche, publiés ou non, émanant des établissements d'enseignement et de recherche français ou étrangers, des laboratoires publics ou privés.

Computational and robotic modeling reveal parsimonious combinations of interactions between individuals in schooling fish

Liu Lei^{1,2}, Ramón Escobedo², Clément Sire³, Guy Theraulaz^{2,*}

1 University of Shanghai for Science and Technology, Shanghai, China

2 Centre de Recherches sur la Cognition Animale, Centre de Biologie Intégrative, Centre National de la Recherche Scientifique (CNRS), Université de Toulouse – Paul Sabatier (UPS), Toulouse, France

3 Laboratoire de Physique Théorique, CNRS and Université de Toulouse – Paul Sabatier, Toulouse, France

* guy.theraulaz@univ-tlse3.fr

Abstract

Coordinated motion and collective decision-making in fish schools result from complex interactions by which individuals integrate information about the behavior of their neighbors. However, little is known about how individuals integrate this information to take decisions and control their motion. Here, we combine experiments with computational and robotic approaches to investigate the impact of different strategies for a fish to interact with its neighbors on collective swimming in groups of rummy-nose tetra (*Hemigrammus rhodostomus*). By means of a data-based agent model describing the interactions between pairs of *H. rhodostomus* (Calovi *et al.*, 2018), we show that the simple addition of the pairwise interactions with two neighbors quantitatively reproduces the collective behavior observed in groups of five fish. Increasing the number of interacting neighbors does not significantly improve the simulation results. Remarkably, and even without confinement, we find that groups remain cohesive and polarized when each agent interacts with only one of its neighbors: the one that has the strongest contribution to the heading variation of the focal agent, dubbed as the “most influential neighbor”. However, group cohesion is lost when each agent only interacts with its nearest neighbor. We then investigate by means of a robotic platform the collective motion in groups of five robots. Our platform combines the implementation of the fish behavioral model and a control system to deal with real-world physical constraints. A better agreement with experimental results for fish is obtained for groups of robots only interacting with their most influential neighbor, than for robots interacting with one or even two nearest neighbors. Finally, we discuss the biological and cognitive relevance of the notion of “most influential neighbors”. Overall, our results suggest that fish have to acquire only a minimal amount of information about their environment to coordinate their movements when swimming in groups.

Keywords: collective behavior; flocking; fish school; interaction networks; computational modeling; collective robotics.

28 Author Summary

29 How do fish integrate and combine information from multiple neighbors when swimming
30 in a school? What is the minimum amount of information about their environment
31 needed to coordinate their motion? To answer these questions, we combine experiments
32 with computational and robotic modeling to test several hypotheses about how individual
33 fish could integrate and combine the information on the behavior of their neighbors
34 when swimming in groups. Our research shows that, for both simulated agents and
35 robots, using the information of two neighbors is sufficient to qualitatively reproduce the
36 collective motion patterns observed in groups of fish. Remarkably, our results also show
37 that it is possible to obtain group cohesion and coherent collective motion over long
38 periods of time even when individuals only interact with their most influential neighbor,
39 that is, the one that exerts the most important effect on their heading variation.

40 Introduction

41 One of the most remarkable characteristics of group-living animals is their ability to
42 display a wide range of complex collective behaviors and to collectively solve problems
43 through the coordination of actions performed by the group members [1–3]. It is now well
44 established that these collective behaviors are self-organized and mainly result from local
45 interactions between individuals [4, 5]. Thus, to understand the mechanisms that govern
46 collective animal behaviors, we need to decipher the interactions between individuals, to
47 identify the information exchanged during these interactions and, finally, to characterize
48 and quantify the effects of these interactions on the behavior of individuals [6, 7]. There
49 exists today a growing body of work that brought detailed information about the direct
50 and indirect interactions involved in the collective behaviors of many animal groups,
51 especially in social insects such as ants [8–11] and bees [12, 13].

52 Recently, we introduced a new method to disentangle and reconstruct the pairwise
53 interactions involved in the coordinated motion of animal groups such as fish schools,
54 flocks of birds, and human crowds [14, 15]. This method leads to explicit and concise
55 models which are straightforward to implement numerically. It still remains an open
56 and challenging problem to understand how individuals traveling in groups combine the
57 information coming from their neighbors to coordinate their own motion.

58 To answer this question, one first needs to identify which of its neighbors an individual
59 interacts with in a group, *i.e.*, which are its influential neighbors. For instance, does an
60 individual always interact with its nearest neighbors, and how many? Most models of
61 collective motion in animal groups generally consider that each individual is influenced by
62 all the neighbors located within some spatial domain centered around this individual [16,
63 17]. This is the case in particular of the Aoki-Couzin model [18, 19] and the Vicsek
64 model [20]. In the latter, each individual aligns its direction of motion with the average
65 direction of all individuals that are located within a fixed distance in its neighborhood.
66 Other models, more directly connected to biological data, consider that the interactions
67 between individuals are topological and that the movement of each individual in the
68 group only relies on a finite number of neighbors. This is in particular the case for the
69 work on starling flocks [21, 22] and on barred flagtails (*Kuhlia mugil*) [23]. In golden
70 shiners (*Notemigonus crysoleucas*), another work has sought to reconstruct the visual
71 information available to each individual fish during collective evasion maneuvers [24].
72 In this species, it has been shown that the transmission of behavior in a school was
73 best described by a model in which the response probability of a fish depends on the
74 fraction of active neighbors perceived by that fish. However, because of the cognitive
75 load that is required for an individual to constantly monitor the movements of a large
76 number of neighbors, it has been suggested that animals may focus their attention on

77 a small subset of their neighbors [25–27]. In a previous work, we found experimental
 78 evidence that supports this assumption. In groups of rummy nose tetras (*Hemigrammus*
 79 *rhodostomus*) performing collective U-turns, we found that, at any time, each fish pays
 80 attention to only a small subset of its neighbors, typically one or two, whose identity
 81 regularly changes [28]. However, we still do not know if the same pattern of interaction
 82 holds true when fish are schooling, *i.e.*, when individuals are moving together in a highly
 83 polarized manner and not performing some collective maneuver.

84 Once the influential neighbors of a focal fish have been identified, one must then
 85 understand how this individual combines the information about the behavior of these
 86 neighbors. The most common assumption is that animals respond by averaging pairwise
 87 responses to their neighbors (with added noise) [16–18]. However, existing work shows
 88 that the integration of information might be much more complex. In golden shiners,
 89 Katz *et al.* [29] have shown that the combined effect of two neighbors on a fish response
 90 is close to averaging for turning, but somewhere between averaging and adding for speed
 91 adjustments. This observation brings us back to an often neglected factor which is the
 92 impact of the physical constraints imposed on a fish movement by their body. Fish
 93 mainly achieve collision avoidance through the control of their speed and orientation
 94 at the individual level. However, existing models seldom treat collision avoidance in a
 95 physical way and most models assume that individuals move at a constant speed [6].
 96 This is the main reason why these models cannot be directly implemented in real physical
 97 robotic systems [30].

98 To better understand how individuals integrate and combine interactions with their
 99 neighbors in a group of moving animals, we first analyze the dynamics of collective
 100 movements in groups of five *H. rhodostomus* moving freely in a circular tank. Then,
 101 we investigate different strategies for combining pairwise interactions between fish
 102 and analyze their impact on collective motion. To do that, we use the data-driven
 103 computational model developed by Calovi *et al.* [14] that describes the interactions
 104 involved in the coordination of burst-and-coast swimming in pairs of *H. rhodostomus*,
 105 and a robotic platform that also allows us to investigate the impact of direction and
 106 speed regulation, and of collision avoidance. Finally, we compare the predictions of the
 107 computational and robotics models with the experiments conducted under the same
 108 conditions with groups of fish.

109 Results

110 We collect three sets of data corresponding to *i*) our experiments with $N = 5$ fish
 111 (*H. rhodostomus*), *ii*) our numerical simulations of the model derived in [14], and *iii*) our
 112 experiments using the robotic platform with $N = 5$ robots (see Fig. 1, S1 Video and
 113 S2 Video), from which we extract the trajectories of each individual (S3 Video). We
 114 characterize the collective behavior of fish, agents, and robots by means of five main
 115 quantities:

- 116 • the group cohesion $C(t)$ at time t , which characterizes the effective radius of the
 117 group, and hence its compactness;
- 118 • the group polarization $P(t)$, which quantifies the coordination of the headings of
 119 the individuals ($P(t) = 1$, if all individuals are perfectly aligned; $P \sim 1/\sqrt{N}$, if
 120 the N individuals have uncorrelated headings, P becoming small only for large
 121 group size N , but being markedly lower than 1 for any $N \geq 5$);
- 122 • the distance $r_w^B(t)$ of the barycenter B of the group from the wall of the tank,
 123 which is only small compared to the radius of the tank if individuals move together
 124 *and* along the wall of the tank;

- 125 • the relative orientation $\theta_w^B(t)$ of the barycenter of the group with respect to the
126 wall of the tank, which in particular characterizes whether the group is collectively
127 swimming parallel to the wall of the tank (then, $|\theta_w^B| \approx 90^\circ$);
- 128 • the counter-milling index $Q(t)$, which measures the relative direction of rotation of
129 individuals inside the group (around the barycenter) with respect to the direction
130 of rotation of the group around the center of the tank (see S4 Video).

131 The Materials and Methods section and Figs. 2 and 3 provide the precise mathematical
132 definition of these quantities. Moreover, we used the Hellinger distance (see Materials
133 and Methods) between two probability distribution functions (PDF) in order to quantify
134 the (dis)similarity between PDF obtained in fish experiments and the corresponding
135 PDF obtained in the fish model (see Table 1) and in robot experiments (see Table 2)

136 *H. rhodostomus* presents a burst-and-coast swimming mode, where a fish suddenly
137 accelerates along a new direction (“kick”; see Fig. 1B, and S1 Video and S3 Video)
138 and then glides passively until the next kick, along an almost straight line, a gliding
139 phase during which the speed approximately decays exponentially [14]. The fish model
140 derived in [14] explicitly implements this swimming mode and returns as the main
141 information the new heading direction of the focal fish after each kick, which is controlled
142 by its environment (wall of the tank, another fish). The interaction between a fish
143 and the wall, and the interaction between two fish have been precisely extracted from
144 actual experiments with *H. rhodostomus* [14]. The original procedure for extracting the
145 interactions introduced in [14] exploited a large data set of ~ 300000 kicks for one-fish
146 trajectories (in tanks of 3 different radii) and ~ 200000 kicks for two-fish trajectories,
147 amounting effectively to a total of 70 hours of exploitable data. The measured interactions
148 were then directly implemented in the model, which is hence not just a phenomenological
149 model with mere guessed, albeit reasonable, interactions. Note however that the analysis
150 in [14] does not provide any insight about how these interactions are combined in groups
151 of more than two fish.

152 The interaction between two fish was shown to be a combination of a repulsive (at
153 short distance of order 1 BL – body length) and a long-range (in particular, compared to
154 zebrafish [15]) attractive interaction at larger distance, and of an alignment interaction
155 which tends to make the two fish align their heading direction. The attraction and
156 alignment interaction functions determine the new heading angle of the focal fish in
157 terms of the instantaneous relative state of the two fish, characterized by the distance
158 between them, the viewing angle with which the neighbor is perceived by the focal fish,
159 and their relative orientation (see Fig. 2). The additional change in heading angle due
160 to the repulsive interaction between a fish and the wall of a circular tank is expressed in
161 terms of the distance and relative angle of the fish to the wall (see Fig. 2). Finally, in
162 addition to the fish-wall and fish-fish interactions, the change in heading angle includes
163 a stochastic contribution describing the spontaneous fluctuations in the motion of the
164 fish. In [14], the model was shown to quantitatively reproduce many fine measurable
165 quantities in one-fish and two-fish experiments, ultimately producing a very precise
166 description of the motion of one or two fish. For the sake of completeness, the model
167 and its fish-wall and fish-fish interaction functions are summarized in the Materials and
168 Methods section (Eqs. (4–15); see [14] for a more detailed description and justification
169 of the model; see [14, 15] for the extraction procedure of the interactions).

170 When more than two fish are swimming in the tank ($N > 2$), the social pairwise
171 interactions must be combined. In the framework of the fish model, it is natural to assume
172 that the heading angle change of a focal fish is the sum of the pairwise contributions of
173 *some* of its $N - 1$ neighbors. The resulting interaction thus depends on two factors: the
174 *number* k of considered neighbors and the *strategy* to select them.

175 We explore three different strategies of interaction between individuals and their
176 neighbors in groups of size $N = 5$, comparing actual fish experiments with the resulting

177 fish model and the robotic platform. In the latter, the robots are programmed with the
 178 fish model and a control procedure to resolve collisions. The first strategy is based on
 179 the *distance*, so that individuals interact with their k nearest neighbors, with $k = 1, 2, 3$.
 180 The second strategy is a *random* strategy, where the k neighbors are randomly sampled
 181 among the other $N - 1$ individuals. Finally, the third strategy is based on the *influence*,
 182 defined below, where the k selected neighbors are those having the largest influence on
 183 the focal individual (as determined by the precise two-fish model of [14]). We also study
 184 the cases where there is no interaction between individuals ($k = 0$), and where each
 185 individual interacts with all its neighbors ($k = 4$).

186 The *influence* $\mathcal{I}_{ij}(t)$ of a neighbor j on a focal individual i at time t is defined as the
 187 intensity of the contribution of this neighbor j to the instantaneous heading variation
 188 of the focal individual i , as given by the firmly tested two-fish model of [14]. The
 189 influence $\mathcal{I}_{ij}(t)$ depends on the relative state of the neighbor j with respect to the focal
 190 individual i , determined by the triplet $(d_{ij}, \psi_{ij}, \phi_{ij})$, where d_{ij} is the distance between
 191 individuals i and j , ψ_{ij} is the viewing angle with which i perceives j (*i.e.*, the angle
 192 between the velocity of i and the vector $\vec{i}j$), and ϕ_{ij} is the difference of their heading
 193 angles, a measure of the alignment between i and j (see Fig. 2). The influence $\mathcal{I}_{ij}(t)$ is
 194 evaluated at each kicking time of individual i by means of the analytical expressions of
 195 the pairwise interaction functions derived in [14] for fish swimming in pairs, according
 196 to Eq. (9) in the Materials and Methods section.

197 To prevent cognitive overload, a reasonable assumption is that individual fish filter
 198 the information from their environment and thus limit their attention to a small set of
 199 their most salient neighbors [25–27] (to be followed; or to be avoided, by moving away
 200 or by aligning their headings), making the notion of most influential neighbors quite
 201 natural.

202 The model for $N > 2$ agents thus proceeds as follows: at the time when the agent
 203 performs a new kick, its change in heading angle is calculated by adding the effects of
 204 the wall and the spontaneous noise to the effects of the k neighbors selected among the
 205 other $N - 1$ individuals according to one of the three strategies presented above:

- 206 • by calculating the instantaneous distance between the focal individual i and each
 207 of its $N - 1$ neighbors and selecting the k nearest neighbors (strategy 1; NEAREST);
- 208 • by randomly sampling k individuals among the $N - 1$ neighbors of i (strategy 2;
 209 RANDOM);
- 210 • by calculating the instantaneous influence $\mathcal{I}_{ij}(t)$ for each neighbor j of i and
 211 selecting the k neighbors with the largest influence (strategy 3; MOST INFLUENTIAL).

212 The strategy is thus characterized by the number k of neighbors taken into account in
 213 the social interaction and the criterion used to select them (NEAREST, RANDOM, or MOST
 214 INFLUENTIAL). The strategy remains unchanged along the whole simulation. However,
 215 the identity of the neighbors selected to interact with a given agent can change from one
 216 kick to another, and must be updated at each kicking time of this agent. For instance,
 217 when using the NEAREST strategy with $k = 2$ in a group of $N = 5$ agents, the agents
 218 taken into account in the social interaction in the n -th kick of agent 1 can be the agents 2
 219 and 3, and the agents 4 and 3 in its $(n + 1)$ -th kick. In order to select these k neighbors at
 220 a specific kick, the $N - 1$ agents must be sorted according to the criterion corresponding
 221 to the strategy used in the simulation. This sorting process is carried out at each kicking
 222 time of the focal agent, independently of the state (kicking or gliding) of the other agents.
 223 If N is so large that the computational cost of this process becomes prohibitive, a more
 224 efficient algorithm can be implemented, such as keeping track of the agents that were
 225 selected in the most recent kicks and exploiting grid algorithms to identify neighbors.

226 These interaction strategies explore different ways for an individual to focus its
 227 attention on the most relevant stimuli (*i.e.*, neighbors).

228 **Collective behavior in fish experiments**

229 Fish form cohesive groups with an average cohesion $C \approx 5$ cm (Fig. 4). They are highly
 230 polarized, with the 5 fish swimming almost in the same direction (large peak at $P \approx 1$
 231 in the distribution of P ; Fig. 5). In some instances, groups are observed in which
 232 one fish swims in the opposite direction to that of the other four, as shown by the
 233 small bump at $P \approx 0.6$ in Fig. 5. Indeed, in this situation, the polarization is close
 234 to $P \approx |1 + 1 + 1 + 1 - 1|/5 = 0.6$. Even less frequent are situations where two fish
 235 swim in the opposite direction to that of the other three, as shown by the very small
 236 bump near $P \approx |1 + 1 + 1 - 1 - 1|/5 = 0.2$. The density maps of polarization P with
 237 respect to cohesion C (panels labeled “FISH” in S1 Fig–S4 Fig) allow to visualize the
 238 correlations between both quantities, and will permit a comparison with the predictions
 239 of the fish model and the results of the robot experiments for the three interaction
 240 strategies considered here.

241 Groups of 5 fish rotate clockwise (CW) or counter-clockwise (CCW) along the tank
 242 wall for long periods and remain close to the border of the tank, the group barycenter
 243 being at a typical distance $r_w^B \approx 7$ cm from the wall (Fig. 6). Therefore, the group swims
 244 almost always parallel to the nearest wall, with a relative angle to the wall of the heading
 245 of the barycenter close to $|\theta_w^B| \approx 90^\circ$ (Fig. 7). In fact, the peak in the PDF of $|\theta_w^B|$ is
 246 slightly below 90° , since the fish are more often going toward the wall than away from
 247 it [14].

248 We also find a collective pattern where individual fish rotate around the barycenter B
 249 of the group in a direction which is *opposite* to the direction of rotation of the group around
 250 the center T of the tank (see Fig. 3 and S4 Video). We call this collective movement a
 251 *counter-milling behavior*, and define the instantaneous degree of counter-milling $Q(t)$ as
 252 a measure in $[-1, 1]$ of the intensity with which both rotation movements are in opposed
 253 directions (see the Materials and Methods section for the precise mathematical definition
 254 of $Q(t)$ and its general interpretation). When $Q(t) < 0$, the fish rotate around their
 255 barycenter B in the opposite direction to that of the group around T (*counter-milling*),
 256 while when $Q(t) > 0$, the fish rotate in the same direction around B as the group rotates
 257 around T (*super-milling*). Fig. 8 shows that the fish exhibit a counter-milling behavior
 258 much more frequently than a super-milling behavior. Counter-milling behaviors result
 259 from the fact that fish located at the front of the group have to reduce their speed as
 260 they get closer to the wall of the tank. Fish located at the back of the group (that
 261 are generally farther from the wall [14]) move faster and outrun the slowing down fish,
 262 ultimately relegating them to the back of the group. This process gives rise to the
 263 rotation of individual fish around the group center, in the opposite direction to the one
 264 that the group displays around the tank (Fig. 3). This collective behavior resembles a
 265 coordinated swimming by relays which is nevertheless due to simple physical constraints,
 266 as already reported on wolf-packs hunting preys moving in circles [31].

267 **Simulation results of the computational model**

268 **Collective motion in a circular tank**

269 Panels (ABC) of Figs. 4–8 show the probability distribution functions for our 5 quantifiers
 270 as obtained in numerical simulations of the fish model. The panels correspond respectively
 271 to the strategy in which agents interact with their k nearest neighbors (A), with
 272 k neighbors chosen randomly (B), and with k neighbors selected according to their
 273 influence on the focal agent (C). For these three strategies (NEAREST; RANDOM; MOST
 274 INFLUENTIAL), we have considered all the possible values of the number of interacting
 275 neighbors, $k = 1, 2, 3$, together with the case where there is no interaction between
 276 agents ($k = 0$) and the case where each agent interacts with every other agent ($k = 4$).

277 For comparison purposes, we have rescaled the distance corresponding to the model
 278 by a factor $\lambda_M = 0.87$. This value is the minimizer of the l_1 -norm of the difference
 279 between the PDF of group cohesion for fish data, and the PDF of group cohesion for the
 280 simulation data produced by the model when using the strategy involving the $k = 2$ most
 281 influential neighbors. Noticeably, the fact that the value of λ_M is close to 1 indicates
 282 that the model produces a quite satisfactory quantitative approximation to the data of
 283 real fish. This rescaling procedure only affects the PDF of C and r_w^B , and not the PDF
 284 of P , θ_w^B , and Q (3 quantities invariant by a change of distance scale).

285 When $k = 0$, there is no interaction between agents and, as expected, one does not
 286 observe any compact group: individuals turn independently around the tank remaining
 287 close and parallel to the wall (as expected for fish swimming alone [14]). Their position
 288 and rotation direction along the walls are uncorrelated, and the individuals are scattered
 289 along the border (cohesion peaked around $C \approx 18$ cm; $r_w^B \approx 15$ cm), with an almost flat
 290 PDF for θ_w^B (random orientation of the barycenter with respect to the wall). This results
 291 in a bell-shaped probability distribution function PDF for the polarization P , vanishing
 292 at $P = 1$ (Figs. 4–7).

293 For $k = 1$, whatever the strategy used to select the interacting neighbor (the nearest
 294 one; a randomly selected one; the most influential one), the dynamics immediately
 295 reveals that interactions are at play, with groups becoming more cohesive (Fig. 4) and
 296 more polarized (Fig. 5) than for $k = 0$. Yet, the NEAREST strategy still leads to a very
 297 broad PDF of the group cohesion C , with a substantial weight near the maximal value
 298 of $C \sim 20$ cm obtained for $k = 0$, indicating that the group often breaks into parts. For
 299 the RANDOM and MOST INFLUENTIAL strategies, the weight at large distance in the PDF
 300 of C is absent, but the PDF are still broader than in fish experiments. As confirmed by
 301 the Hellinger distance quantifier (see Table 1 and Materials and Methods), the MOST
 302 INFLUENTIAL strategy clearly leads to the sharper distribution of C (peaked around
 303 $C \approx 6.5$ cm, compared to $C \approx 10$ cm for the RANDOM strategy). The next section will
 304 show that, contrary to the NEAREST strategy, the MOST INFLUENTIAL strategy with
 305 $k = 1$ can lead to compactness of the group even for larger groups ($N = 6–70$) moving
 306 in an *unbounded* domain. As for the group polarization P (Fig. 5), the three strategies
 307 lead to a PDF clearly peaked near $P \approx 0.9$ (and a smaller peak near $P \approx 0.6$; see above),
 308 yet certainly not as peaked near $P = 1$ as the PDF for fish experiments. Again, the
 309 MOST INFLUENTIAL strategy leads to the best agreement with fish experiments (see
 310 Table 1), although the difference between strategies is not as marked as for the group
 311 cohesion. For the three strategies, the barycenter of the group is closer to the border
 312 and moves more parallel to the wall (Figs. 6 and 7). Counter-milling is obtained for
 313 the three strategies with comparable PDF (Fig. 8; see also S5 Fig), quite similar to the
 314 one obtained in fish experiments (we will see that the agreement unfortunately worsens
 315 when increasing k ; see Table 1). Polarization vs cohesion density maps confirm that the
 316 NEAREST and RANDOM strategies are insufficient to convey the necessary information to
 317 reach the degree of cohesion and polarization (and their correlation) observed in groups
 318 of fish (S1 Fig, S2 Fig). The MOST INFLUENTIAL strategy density maps for $k = 1$ already
 319 present the main features of the fish experiments, despite a still too broad spreading
 320 in the (C, P) plane. Overall, for $k = 1$, the MOST INFLUENTIAL strategy gives rise to
 321 significantly better results than the NEAREST and RANDOM strategies (see Table 1).

322 For $k = 2$, the three strategies lead to a collective behavior in much better agreement
 323 with the fish experiments (see Table 1). In particular, the NEAREST strategy now system-
 324 atically leads to compact groups, with a PDF of the group cohesion C (Fig. 4) similar
 325 to the one obtained for the RANDOM strategy (both peaked around $C \approx 6.5$ cm). The
 326 MOST INFLUENTIAL strategy produces a PDF in good agreement with fish experiments
 327 (both sharply peaked around $C \approx 5$ cm). The PDF of the polarization is now sharply
 328 peaked at $P = 1$ for the three strategies, with a slightly lower level of polarization for

329 the RANDOM strategy compared to the two others (see Fig. 5 and Table 1). Like in the
 330 case $k = 1$, the distance and alignment of the group with respect to the wall are better
 331 recovered for the NEAREST strategy (Figs. 6 and 7; Table 1), the two other strategies
 332 leading to slightly broader PDF but much narrower compared to the case $k = 1$. The
 333 counter-milling Q is enhanced for the three strategies compared to the case $k = 1$ and
 334 appears stronger than for fish experiments (Fig. 8). The deterioration of the model
 335 results for the counter-milling compared to $k = 1$ and experiments suggests that the
 336 internal structure of a fish group is more rigid than predicted by the model, actual fish
 337 behaving closer to particles rotating on a vinyl record (see the interpretation of Q in
 338 Materials and Methods). Compared to the case $k = 1$, where they were particularly far
 339 from the experimental maps, polarization vs cohesion density maps for the NEAREST
 340 and RANDOM strategies and $k = 2$ show a correlation between P and C in much better
 341 agreement with experiments (S1 Fig, S2 Fig). The MOST INFLUENTIAL strategy results,
 342 already fair for $k = 1$, also improve. The NEAREST strategy leads to the best agreement
 343 with experiments in the representation of S1 Fig, while the MOST INFLUENTIAL strategy
 344 leads to the best results in the representation of S2 Fig.

345 When interacting with $k = 3$ neighbors, the results are almost identical for the
 346 three strategies because neighbors are the same a high percentage of the time. For two
 347 (respectively, three) given strategies, the selected neighbors are exactly the same 25% of
 348 the time (respectively, 6.25%); they have at least 2 neighbors in common 75% of the
 349 time (respectively, 93.75%); there is always at least one neighbor in common. Interacting
 350 with the 3 nearest neighbors instead of 2 only improves the group cohesion (see Table 1
 351 and Fig. 4), while using the 3 most influential ones, instead of 2, does not improve
 352 significantly any of the measures, including density maps (S1 Fig, S2 Fig). As already
 353 noted for $k = 2$, the counter-milling remains too pronounced compared to experiments
 354 for the three strategies and $k = 3$ (see Fig. 8 and S5 Fig).

355 Finally, interacting with $k = 4$ neighbors does not significantly change the results
 356 obtained for $k = 3$ (see Figs. 4–8 and Table 1).

357 Collective motion of 5 agents in an unbounded domain

358 The model allows us to simulate the condition where agents are swimming in an un-
 359 bounded domain by removing the interaction with the wall. This condition is particularly
 360 interesting to assess the impact of the confinement of the agents due to the arena on
 361 group cohesion and polarization.

362 Figs. 9 and 10 show respectively the time evolution of group cohesion and polarization
 363 for the MOST INFLUENTIAL strategy (Panels AD) and the NEAREST strategy (Panels BE),
 364 and for $k = 1$ to 4. Despite the absence of confinement due to the wall, all the strategies
 365 except the one that consists in interacting only with the nearest neighbor ($k = 1$) allow
 366 the group to remain cohesive and polarized for more than 2.5 hours ($\approx 10^4$ kicks) in
 367 numerical simulations (see Figs. 9ABC and 10AB). When agents only interact with their
 368 most influential neighbor, the group is highly cohesive ($C \approx 0.1$ m, Fig. 9A), but less
 369 than in the arena ($C \approx 0.07$ m, Fig. 4C). However, the polarization is higher when the
 370 group swim in an unbounded domain (mean of $P \approx 0.93$, Fig. 10A) in comparison to
 371 the arena (mean of $P \approx 0.78$, Fig. 5C). Therefore, the confinement due to the arena
 372 reinforces the group cohesion and weakens the group polarization, which still remains at
 373 a high level for the MOST INFLUENTIAL strategy.

374 However, when agents only interact with their first nearest neighbor, the group
 375 disintegrates very quickly and then diffuses, with $C^2(t)$ growing linearly with the time t
 376 (Fig. 9C), and $P(t)$ oscillating around 0.6 (Fig. 10B). Compact groups are recovered for
 377 the NEAREST strategy with $k = 2, 3$, but the MOST INFLUENTIAL strategy systematically
 378 leads to more cohesive and more polarized groups (Fig. 9AB).

379 In order to better understand to what extent the group cohesion depends on the

380 interaction strategy and/or on the long-range nature of the attraction [14], we have
 381 also simulated the model by truncating the attraction interaction between two agents i
 382 and j when their distance d_{ij} is greater than a cut-off distance d_{cut} : $F_{\text{Att}}(d_{ij}) = 0$, if
 383 $d_{ij} > d_{\text{cut}}$, where F_{Att} is defined in Eq. (10) of the Materials and Methods section. When
 384 d_{cut} decreases below some critical value d_{cut}^* , we expect that the group will break and
 385 that the agents will ultimately freely diffuse, illustrating the importance of the range
 386 of the attraction interaction to ensure the cohesion of the group (see Fig. 9DE) and
 387 Fig. 10DE).

388 For the MOST INFLUENTIAL strategy with $k = 1$, the group remains highly cohesive
 389 (Fig. 9D) and highly polarized (Fig. 10D) for $d_{\text{cut}} > d_{\text{cut}}^* \approx 0.9$ m. For $k = 2, 3$,
 390 and 4, d_{cut}^* is found to be slightly smaller than for $k = 1$ ($d_{\text{cut}}^* \approx 0.8$ m; Fig. 9D). For
 391 the NEAREST strategy with $k = 2$ (the group is never cohesive for $k = 1$, even for
 392 $d_{\text{cut}} = \infty$; see above), we find $d_{\text{cut}}^* \approx 3.5$ m (Fig. 9E), much higher than for $k = 1$ in the
 393 MOST INFLUENTIAL strategy. Here, we clearly see that even at a smaller k , the MOST
 394 INFLUENTIAL strategy is much more effective than the NEAREST strategy in ensuring
 395 the cohesion of the group, for finite-range attraction cut-off at d_{cut} . For $k = 3$, the
 396 NEAREST strategy leads to a critical cut-off $d_{\text{cut}}^* \approx 0.9$, of the same order as for the MOST
 397 INFLUENTIAL strategy (for $k = 3$, the involved neighbors are often the same for both
 398 strategies; see above).

399 In conclusion, for groups of 5 agents in an unbounded domain, we have shown that
 400 the MOST INFLUENTIAL strategy leads to a highly cohesive and polarized group for all
 401 $k = 1, 2, 3$, provided the range of the attraction is not too small ($d_{\text{cut}} > 0.8$ m). For the
 402 NEAREST strategy, the group is never cohesive for $k = 1$, and a much larger range of the
 403 attraction ($d_{\text{cut}} > 3.5$ m) is required to ensure the cohesion of the group for $k = 2$.

404 Collective motion of larger groups in an unbounded domain

405 For agents moving in an unbounded domain, we have simulated the model with the MOST
 406 INFLUENTIAL strategy with $k = 1$, for groups of $N = 6$ to 70 individuals starting initially
 407 in a compact configuration (see Fig. 10C). The group remains highly cohesive for all sizes
 408 (up to $N = 70$), with a group cohesion of order $C \sim 0.1$ m. The polarization remains
 409 high ($P > 0.7$) in groups of size $N \leq 20$, and decreases as the group size increases. This
 410 suggests a smooth cross-over between a schooling phase up to moderate group sizes
 411 $N \sim 20$, and a more disordered swarming phase for larger N . In fact, for the largest
 412 values of N investigated, schooling periods are also observed, alternating with periods
 413 of collective milling, resulting de facto in a reduced polarization of the group. The
 414 occurrence of the swarming, schooling, and milling phases as a function of the model
 415 parameters (group size N , strategy to select the interacting neighbors, intensity and
 416 range of the attraction/alignment interactions...) will be studied in a future work, as it
 417 has been previously done for the species *Kuhlia mugil* [32] (a species displaying a smooth
 418 swimming mode, instead of a burst-and-coast swimming mode).

419 When agents only interact with their nearest neighbor, groups larger than $N = 5$
 420 disperse immediately and a larger number of neighbors k must be taken into account to
 421 preserve some degree of cohesion. We have also simulated larger groups ($N = 6, \dots, 26$;
 422 N even) with $k = 1$ to $N - 1$ for the NEAREST strategy. The results of S7 Fig (and
 423 Fig. 10F, in the particular case $N = 20$) show that each agent must interact at least
 424 with $k \sim N/2$ nearest neighbors in order to obtain a degree of cohesion similar to the
 425 one observed for the MOST INFLUENTIAL strategy with $k = 1$. Moreover, once $k > N/2$,
 426 groups become less cohesive as the number of nearest neighbors taken into account by
 427 agents increases. In fact, for $N > 6$ and whatever the value of k , the NEAREST strategy
 428 always leads to less cohesive groups (S7 FigA) than for the MOST INFLUENTIAL strategy
 429 with $k = 1$, for which $C \sim 0.1$ m.

430 The simulation results also show that for the NEAREST strategy with $k < 7$, the

431 degree of polarization decreases with the group size. Moreover, the polarization reaches
432 a maximum for $k \sim N/2$ until $N \leq 14$. For larger groups, interacting with more than
433 $k = 7$ nearest neighbors reduces the degree of polarization, which becomes smaller as k
434 increases (see S7 FigB and the particular case of $N = 20$ in Fig. 10F).

435 Collective behavior in robotics experiments

436 We now present the results of a series of experiments with $N = 5$ robots exploiting the
437 three interaction strategies considered in the fish model. The robots are programmed
438 to reproduce the model behavior (Eqs. (4–15) in Materials and Methods), with model
439 parameters adapted to the different spatial and temporal scales of the robotic experi-
440 mental setup (see Table 3). In addition, robots operate a control procedure designed to
441 resolve collisions with the wall, and most importantly, with other robots (see Materials
442 and Methods). Indeed, contrary to point particle agents in the fish model or to real fish
443 swimming in shallow water (a truly 3D environment), robots moving on a strictly 2D
444 setup cannot physically cross each other. The robots hence combine a behavioral model
445 and an engineering-minded control system to deal with real-world physical constraints.
446 Our robotic platform provides a concrete implementation of these two elements and
447 understanding their interplay and their combined impact on the collective behavior of
448 robots is certainly one of the main motivation of the experiments presented here.

449 Panels (DEF) of Figs. 4–8 show the results of the robotic experiments performed in
450 the same conditions as those studied with the model, including the case where robots do
451 not interact with each other ($k = 0$) and the case where each robot interacts with all its
452 neighbors ($k = 4$). However, the robotic experiment for the case $k = 3$ for the MOST
453 INFLUENTIAL strategy was not performed. Counter-milling in robots is illustrated in S6
454 Fig, and the density maps of cohesion and polarization are shown in S3 Fig and S4 Fig.
455 The robotic platform and the monitoring of a group of 5 robots in motion are shown in
456 S2 Video.

457 Despite the fact that the spatial and temporal scales of the robotic platform have
458 been scaled at best to correspond to that of the fish experiments (in particular, 4×4 cm
459 square robots in an arena of radius $R = 42$ cm vs elongated fish of typical length 3 cm
460 swimming in a tank of radius $R = 25$ cm), the border and other robots have a stronger
461 effect on a focal robot at short distance. Indeed, as explained above, the collision
462 avoidance protocol (see Materials and Methods) induces effective interactions between
463 the robots that have a longer range than the interactions between fish. In addition, the
464 square shape of the robot also makes them effectively bigger than if they were elongated
465 like fish. Hence, the rescaling of distances as measured in robot experiments is necessary
466 to be able to compare the different spatial distributions in fish and robot experiments,
467 although it does not affect polarization, counter-milling, or angular distributions. As a
468 result, we found a much smaller scaling factor than in model simulations: $\lambda_R = 0.35$.
469 Note that once the optimal scaling factor is determined, it is kept fixed in all considered
470 situations (strategy to select the interacting neighbors and their number k). From now,
471 all distances in the robot experiments mentioned in this section are hence expressed
472 after rescaling to be comparable to corresponding distances in the fish experiments.

473 When $k = 0$, robots move independently from each other when they are sufficiently
474 far from each other, and tend to remain dispersed along the border of the arena (S5
475 Video). The group cohesion is weak (cohesion peaked at $C \sim 12$ cm; Fig. 4DEF), and
476 the distance of the barycenter to the wall is large ($r_w^B \sim 12$ cm; Fig. 6DEF). Robots are
477 relatively more cohesive and closer to the wall compared to the fish model for $k = 0$ due
478 to volume exclusion effects (two colliding robots can end up going in the same direction
479 as a result of the control procedure) and because the confining effects of the border of
480 the arena are stronger in robots than in agents (see also S3 Fig and S6 Fig). Robots are
481 not polarized, as already observed in the fish model simulations for the same condition

482 $k = 0$ (Panels DEF in Figs. 5).

483 Interacting only with $k = 1$ nearest neighbor does not allow robots to coordinate their
 484 motion and move as a coherent group (see S6 Video). Panel (D) of Figs. 4–8 (cohesion;
 485 polarization; distance to the wall; angle with respect to the wall; counter-milling) show
 486 that the results for $k = 1$ are similar to those obtained for $k = 0$, with a marginal
 487 improvement of the group cohesion and polarization. On the other hand, when the
 488 robots interact with their most influential neighbor (S7 Video), the group is highly
 489 cohesive ($C \sim 6.5$ cm; Fig. 4F) and highly polarized (large peak at $P = 1$ in Fig. 5F).
 490 The robots collectively move close to the border ($r_w^B \sim 7$ cm; Fig. 6F). Counter-milling is
 491 also clearly visible (Fig. 8F, S7 Video and S6 Fig). Moreover, for the RANDOM strategy
 492 with $k = 1$, the results are somewhat intermediate between those for the NEAREST and
 493 MOST INFLUENTIAL strategies, in terms of cohesiveness, polarization, and counter-milling
 494 (see Panel E in Figs. 4, 5, 8 respectively, and S8 Video). The similarity of the density
 495 maps of cohesion and polarization with those found in fish experiment is the highest for
 496 the MOST INFLUENTIAL strategy compared to the other two strategies (S3 Fig and S4
 497 Fig). Overall, and as confirmed by the Hellinger distances listed in Table 2, the MOST
 498 INFLUENTIAL strategy with $k = 1$ produces highly cohesive and polarized robot groups
 499 leading to a qualitative agreement with fish experiments, whereas the NEAREST strategy
 500 does not even lead to any significant group coordination.

501 Extending the interaction to the $k = 2$ nearest neighbors reinforces group coordination
 502 (S9 Video): groups are more cohesive (the peak in the PDF of C decreases from around
 503 10 cm for $k = 1$, to 7 cm), and simultaneously more polarized (S3 Fig). However, the
 504 polarization remains weak compared to fish experiments, and even compared to the
 505 MOST INFLUENTIAL strategy for $k = 1$: the PDF of P has a wide region of high values
 506 centered in $P \approx 0.85$ and is not peaked at $P = 1$ (Fig. 5D). The high peak at $P = 0.6$
 507 reveals that situations in which groups of 4 robots move in the same direction while the
 508 fifth robot moves in the opposite direction are quite frequent. Wide groups ($C > 8$ cm,
 509 Fig. 4D) moving far from the border ($r_w^B > 9$ cm, Fig. 6D) are still frequent, and
 510 counter-milling is still barely visible (S6 Fig). On the other hand, interacting with the
 511 two most influential neighbors definitively produces patterns that are similar to those
 512 observed in fish experiments, especially if we consider the polarization, where the peak
 513 at $P = 1$ clearly narrows and doubles its height (Fig. 5F and S10 Video), although the
 514 improvement with respect to the MOST INFLUENTIAL strategy with $k = 1$ is small, or
 515 even negligible, if we consider the counter-milling index (Fig. 8F). Again, the RANDOM
 516 strategy with $k = 2$ leads to an overall much better agreement with fish experiments
 517 than the NEAREST strategy with $k = 2$ (see Hellinger distances between PDF in Table 2).
 518 Except for the weaker polarization, the results for the RANDOM strategy are similar to
 519 the ones obtained for the MOST INFLUENTIAL strategy with $k = 2$ (see Table 2 and S11
 520 Video).

521 For $k = 3$, the results for the NEAREST strategy (see S12 Video) improve drastically
 522 and are in comparable agreement with fish experiments as the results for the RANDOM
 523 strategy (S13 Video), and on par with those for the MOST INFLUENTIAL strategy for
 524 $k = 1, 2$ (see Table 2). For the NEAREST and RANDOM strategies (sharing 2, and often
 525 3, common neighbors for $k = 3$), groups are highly cohesive (Fig. 4DE) and polarized
 526 (Fig. 5DE), with a narrower PDF of C than in fish experiments, pointing to the robot
 527 groups having less internal fluctuations than fish groups. Accordingly, the PDF of r_w^B
 528 (Fig. 6DE) is peaked at the same value as in fish experiments, $r_w^B \approx 5.5$ cm, but is again
 529 narrower, with much less weight at distances $r_w^B > 8$ cm. The PDF of θ_w^B (Fig. 6DE) is in
 530 good agreement with fish experiments, and counter-milling is clearly obtained (S6 Fig).
 531 When robots interact with $k = 4$ neighbors (S14 Video), the results are very similar to
 532 the case $k = 3$ within the non negligible statistical fluctuations due to our shorter robot
 533 experiments compared to the fish experiments and fish model simulations.

534 In conclusion, many of the results of the robotic experiments are qualitatively similar
 535 to those found in the simulations of the model, despite the robots being submitted
 536 to real-world physical constraints. Yet, for robots, the MOST INFLUENTIAL strategy
 537 with $k = 1$ is found to lead to cohesive and polarized groups (like in the model), while
 538 the NEAREST strategy with $k = 1$ does not lead to any significant group coordination
 539 (weaker coordination for the model in a confining domain, but no cohesive groups in an
 540 unbounded domain).

541 Discussion

542 Collective motion involving the coherent movements of groups of individuals is primarily
 543 a coordination problem. Each individual within a group must precisely adjust its
 544 behavior to that of its neighbors in order to produce coordinated motion. Determining
 545 how these relevant neighbors are selected at the individual scale is therefore a key
 546 element to understand the coordination mechanisms in moving animal groups. Previous
 547 experimental works on fish and birds have identified interacting neighbors using short-
 548 term directional correlations [17,34] or anisotropy of the position of the nearest neighbors
 549 [21]. In a starling flocks (*Sturnus vulgaris*), each bird coordinates its motion with a finite
 550 number of closest neighbors (typically seven), irrespective of their distance [21]. However,
 551 in fish schools, experimental studies suggest that each individual only interacts with a
 552 smaller number of influential neighbors. For instance, in the mosquitofish (*Gambusia*
 553 *holbrooki*), each fish mostly interacts with a single nearest neighbor [35]. In the rummy
 554 nose tetra (*Hemigrammus rhodostomus*) during collective U-turns [28,36], the analysis
 555 of directional correlations between fish suggests that each fish mainly reacts to one or
 556 two neighbors at a time [28]. These results are in line with theoretical works that have
 557 suggested that, instead of averaging the contributions of a large number of neighbors,
 558 as suggested by many models [18–20,23,37,38], individuals could pay attention to only
 559 a small number of neighbors [25–28,39]. This mechanism would overcome the natural
 560 cognitive limitation of the amount of information that each individual can handle [33].

561 Here, we addressed this question in groups of five *H. rhodostomus* swimming in a
 562 circular tank. This species of fish is of particular interest because of its tendency to form
 563 highly polarized groups and its burst-and-coast swimming mode [14], which allows us to
 564 consider that each fish adjusts its heading direction at the onset of each bursting phase,
 565 that is labeled as a “kick”. Just before these brief accelerations, a fish integrates and
 566 filters the information coming from its environment and picks its resulting new heading.

567 In our experiments, groups of five fish remain highly cohesive, almost perfectly
 568 polarized, and swim along and close to the wall of the tank, keeping the same direction of
 569 rotation for very long periods [36]. Fish groups also display a remarkable counter-milling
 570 collective behavior where individual fish rotate around the group barycenter in the
 571 opposite direction to that of the group in the tank, so that individuals alternate their
 572 positions at the front of the group.

573 Based on a previous work in which we have reconstructed and modeled the form of the
 574 interactions of *H. rhodostomus* fish swimming in pairs [14], we analyzed three strategies
 575 for combining the pairwise interactions between a focal fish and a number $k = 1$ to 3 of
 576 its neighbors by means of a computational model and a robotic platform. In the NEAREST
 577 strategy, neighbors are selected according to their distance to the focal individual. In
 578 the RANDOM strategy, neighbors are randomly chosen, and in the MOST INFLUENTIAL
 579 strategy, neighbors are selected according to the intensity of their contribution to the
 580 heading variation of the focal individual. The impact of these strategies on the resulting
 581 collective behavior was then measured and analyzed by means of five quantities: group
 582 cohesion, group polarization, distance and relative orientation of the barycenter with
 583 respect to the border of the tank, and counter-milling index.

584 Our results suggest that when individuals (agents or robots) interact with a minimal
 585 number of neighbors, namely two, a group of individuals is able to reproduce the main
 586 characteristics of the collective movements observed in the fish experiments.

587 In the simulations of the model for $N = 5$, when the agents are interacting with
 588 a single neighbor, this immediately leads to the formation of groups. Whatever the
 589 strategy used to select a neighbor, the quantities used to quantify group behavior show
 590 that the exchange of information with a single neighbor leads agents to get closer to each
 591 other, at least temporarily for the NEAREST strategy. However, whatever the strategy
 592 considered, cohesion, polarization, and counter-milling are still weak compared to fish
 593 experiments, although the MOST INFLUENTIAL strategy convincingly leads to the best
 594 group coordination for $k = 1$.

595 The simulations of the model in an unbounded domain show that group cohesion is
 596 maintained over long periods of time when agents only interact with their most influential
 597 neighbor, provided the attraction range is above a critical threshold distance. However,
 598 when agents only interact with their nearest neighbor, this systematically leads to the
 599 diffusive dispersion of the group. For groups of size up to $N = 70$, interacting with the
 600 most influential neighbor leads to compact groups, while one needs to consider typically
 601 at least $\sim N/2$ nearest neighbors to achieve the same result for the NEAREST strategy.
 602 Therefore, the cohesion of the group observed in the arena is not a merely consequence
 603 of the confinement of the agents, but mainly results from the higher quality of the
 604 information provided by the influential neighbors in comparison to the one provided by
 605 the nearest neighbors.

606 Then, when agents acquire more information about their environment ($k = 2$), all
 607 the interaction strategies implemented in the model give rise to collective behaviors that
 608 are in qualitative agreement with those observed in the experiments with fish, and a
 609 quantitative agreement is even reached for some quantities characterizing group behavior
 610 (see Table 1). When agents collect even more information about their environment
 611 (*i.e.*, when they pay attention to $k = 3$ neighbors), the agreement with fish experiments
 612 is not improved if the neighbors are chosen according to their influence. However,
 613 groups become more cohesive and polarized when the agents interact with their nearest
 614 neighbors. Yet, for $k = 3$, the three strategies lead to comparable results, which is
 615 consistent with the facts that two strategies have necessarily at least two common
 616 neighbors for groups of five individuals. Note that for $k = 2$ and $k = 3$, and for all
 617 three strategies, the intensity of the counter-milling is larger in the model than in fish
 618 experiments, suggesting that the internal structure of real fish groups is more rigid than
 619 predicted by the model.

620 In summary, the simulation results clearly indicate that group behaviors similar
 621 to those observed in fish experiments can be reproduced by our model, provided that
 622 individuals interact with at least two of their neighbors at each decision time and no
 623 clear gain is obtained when agents interact with a third additional neighbor. When only
 624 one interacting neighbor is considered, the MOST INFLUENTIAL strategy leads to the
 625 best group coordination, which even survives when the group moves in an unbounded
 626 domain.

627 By implementing the behavioral fish model and the same local interaction strategies
 628 in our robotic platform, we also investigated the impact of the physical constraints and
 629 the collision avoidance protocol based on speed control on the group behavior. The
 630 MOST INFLUENTIAL strategy is much more efficient than the two other strategies to
 631 ensure group cohesion and polarization (see Table 2). Remarkably, and as already
 632 observed in the model simulations, even when robots only interact with their most
 633 influential neighbor, the group remains highly cohesive and polarized, and close to the
 634 border. By contrast, when robots only interact with their nearest neighbor, they are
 635 not able to exhibit any kind of coordinated behavior. Everything happens as if pairwise

636 interactions between robots were screened by the effect induced by the collision avoidance
637 protocol: the distributions of the group cohesion, the polarization, and the distance
638 of the barycenter of the group to the border of the tank are almost identical to those
639 obtained with the null model, in which no interaction exists between robots except for
640 collision avoidance. When robots interact with two neighbors, the agreement with the
641 results of fish experiments is improved, but it is only when robots interact with three
642 nearest neighbors that the NEAREST strategy produces highly cohesive and polarized
643 groups.

644 Overall, and even more convincingly than in the case of the fish model, the MOST
645 INFLUENTIAL strategy leads to the best overall agreement with fish experiments for $k = 1$
646 and $k = 2$, even producing strongly coordinated groups for $k = 1$. Compared to the
647 case of the fish model, the NEAREST strategy does not lead to any significant group
648 coordination for $k = 1$, and only to moderately cohesive and polarized groups for $k = 2$,
649 yet being even less efficient than the RANDOM strategy. The robot collision avoidance
650 protocol induces a strong effective repulsion between close neighbors, which screens the
651 behavioral interactions for the strategy based on these nearest neighbors.

652 Note that implementing the k -MOST INFLUENTIAL strategy in a computational
653 model for larger groups of agents is not more computationally challenging than the
654 implementation of the more common k -NEAREST strategy, and is even less demanding
655 than the consideration of the first layer of neighbors in a Voronoi construction used in
656 many phenomenological flocking models [21, 22, 32]. For very large groups ($N > 10000$),
657 rarely considered in the context of fish models, the implementation of the k -MOST
658 INFLUENTIAL and k -NEAREST strategies could also be optimized by exploiting grid
659 algorithms commonly used in computational physics and astrophysics.

660 However, beyond its purely computational complexity, the possible biological relevance
661 of the MOST INFLUENTIAL strategy (with small k) for fish and potentially other animals
662 is certainly an important question. In vertebrates, and in particular in fish, the midbrain
663 and forebrain networks are carrying out computation in parallel to process the visual
664 information and select the most salient stimuli that are the focus of attention. The
665 midbrain network continuously monitors the environment for behaviorally relevant
666 stimuli [40]. This is a primary site where the information about the neighbors is filtered
667 for cognitive decision. Then, the forebrain network selects those stimuli on which the fish
668 focuses its attention. The interaction strategies that we have investigated in this work
669 correspond to different ways for an individual to focus its attention on the stimuli (*i.e.*,
670 its relevant neighbors). In the context of fish schools, individuals filter the information
671 from their environment and thus limit their attention to a small set of their most salient
672 neighbors [25–27], hence giving priority to the few neighbors to be avoided (by moving
673 away or by aligning their headings) or the ones to be followed. These few neighbors
674 requiring an immediate action from the focal fish should, by definition, trigger a larger
675 response than other neighbors, hence making the notion of most influential neighbors
676 quite natural. Our results show that each fish interacts with typically two neighbors
677 that are the most salient, a process which reduces the amount of information that needs
678 attention and which hence permits to avoid any cognitive overload.

679 In conclusion, each individual must acquire a minimal amount of information about
680 the behavior of its neighbors for coordination to emerge at the group level, thus allowing
681 fish to avoid information overload when they move in large groups [33].

682 **Materials and Methods**

683 **Fish experiments**

684 **Ethics statement.** Our fish experiments have been approved by the Ethics Committee
 685 for Animal Experimentation of the Toulouse Research Federation in Biology N° 1 and
 686 comply with the European legislation for animal welfare.

687 **Study species.** Rummy-nose tetras (*Hemigrammus rhodostomus*) were purchased
 688 from Amazonie Labège (<http://www.amazonie.com>) in Toulouse, France. Fish were kept
 689 in 150l aquariums on a 12:12 hour, dark:light photoperiod, at 25.2 °C (± 0.7 °C) and
 690 were fed *ad libitum* with fish flakes. The average body length of the fish used in these
 691 experiments is 31 mm (± 2.5 mm).

692 **Experimental setup.** We used a rectangular experimental tank of size 120 × 120 cm,
 693 made of glass, supported by a structure of metal beam 20 cm high. A plywood plate
 694 was interposed between the mesh and the basin to dampen the forces exerted on the
 695 glass basin by its own weight and water. This structure also enables the attenuation
 696 of vibrations. The setup was placed in a chamber made by four opaque white curtains
 697 surrounded by four LED light panels to provide an isotropic lighting. A circular tank of
 698 radius $R = 250$ mm was set inside the experimental tank filled with 7 cm of water of
 699 controlled quality (50% of water purified by reverse osmosis and 50% of water treated
 700 by activated carbon) heated at 24.9 °C (± 0.8 °C). Reflection of light due to the bottom
 701 of the experimental tank is avoided thanks to a white PVC layer.

702 Each trial started by placing groups of $N = 5$ fish randomly sampled from the
 703 breeding tank into the circular tank. Fish were let for 10 minutes to habituate before
 704 the start of the trial. A trial then consisted of one hour of fish freely swimming in
 705 the circular tank with experimenters out of the room. Fish trajectories were recorded
 706 by a Sony HandyCam HD camera filming from above the setup at 25 Hz (25 frames
 707 per second) in HDTV resolution (1920×1080p). We performed 11 trials with groups of
 708 $N = 5$ fish, and for each trial, we used different fish taken from the breeding tank.

709 **Robotic platform**

710 **Robots.** We used a robotic platform composed by small compact mobile robots that
 711 we named “Cuboids”, a name chosen in reference to the first realistic computer program
 712 that simulated the flocking behavior in birds and the schooling behavior in fish, called
 713 “Boids”, developed in 1986 by Craig Reynolds [41]. The Cuboids robots were specifically
 714 designed by us for this experiment.

715 Cuboids have a square basis of 40 × 40 mm, they are 60 mm high and weigh 50 g
 716 (Fig. 11). We now describe the elements of a Cuboid (numbers between parentheses
 717 refer to labels in Fig. 11). Each robot is equipped with two differential wheels (7)
 718 driven by small DC motors (13). The small belts (9) connect wheels to the DC motors,
 719 which can drive the robot with a maximum speed of 50 mm/s. The two wheels are
 720 mounted on a central axis (6). An IEEE 802.11n/WIFI module (8) with a range of
 721 approximately 200 m is used for communication network between robot and a wireless
 722 router. A Li-Poly rechargeable battery (15) provided energy for about 6 hours in our
 723 experimental conditions. In addition, a coil (12) located under the robot, can be used
 724 to charge the robot wirelessly while it is working. The charging circuit is located on
 725 the side board (11). The robot bottom hosts a 32-bit, 168 MHz ARM microprocessor
 726 STM32F4 (14), which can provide multi control loops with the time duration up to
 727 2 ms. Besides, another 8-bit microcontroller PIC18F25k22 is mounted on the top sensor
 728 board (1), which controls a LCD screen (16) to display information and a 3-colors

729 LED (17). The microprocessor communicates with the microcontroller by 4 copper
 730 bars (4), which can simultaneously provide power and communication bus.

731 Each Cuboid also has several sensors to measure the relative positions of other robots
 732 in its neighborhood and to send and receive messages from these robots. Within a
 733 sensing range of about 20 cm, a robot can send messages (infrared signals) by the center
 734 IR transmitter (3). There are two IR receivers (2) on both sides of the robots, which
 735 can determine the distance of a neighboring robot that transmits the infrared signal.
 736 From the two distance values provided by the IR receivers, the angle with which this
 737 neighboring robot is perceived by the focal robot can be calculated by triangulation.
 738 Furthermore, the relative position of the neighboring robot to the focal one can be
 739 computed by the information of the distance and the angle of perception acquired before.
 740 On the other side, the IR signal also carries a short message that includes information
 741 on robot ID, orientation angle, speed and states. The heading of a Cuboid is measured
 742 by a motion tracking sensor MPU-9250 (18). This device consists of a 3-Axis gyroscope,
 743 a 3-Axis accelerometer, and a 3-Axis magnetometer. Hence, the MPU-9250 is a 9-axis
 744 Motion Tracking device that also combines a Digital Motion Processor. With its I2C bus
 745 connected with PIC18F25K22, the MPU-9250 can directly provide complete 9-axis
 746 Motion Fusion output to the microcontroller. These sensing and local communication
 747 devices have not been used in the experiments that have been done in a supervised
 748 mode.

749 We tested the model with the robotic platform because there are many physical aspects
 750 that have to be considered to assess the robustness of the coordination mechanisms when
 751 they are implemented in a physical hardware. These physical aspects include the friction
 752 of wheels, the noise of gear box, the blurring of the camera, the wrong identification of
 753 the tracker, the delay of the communication, the overload of computation, the blocking
 754 of the onboard communication bus, the square shape collision of the robot frame, the
 755 mismatch parameters of the interaction model, the impact of the obstacle avoidance
 756 protocol, and the non-holonomic constraint of the robot. All these physical aspects can
 757 have a large effect on the individual and collective behaviors (especially when robots
 758 move in a crowded space) and are difficult to include in a model.

759 **Experimental platform.** The robotic experimental setup consisted of a circular
 760 arena of radius 420 mm resting on a 1×1 m square flat surface with a camera (Basler
 761 piA2400-17gc) mounted on the top (see Fig. 12). The setup was placed in a chamber
 762 made by 3 opaque wooden boards and 1 white curtain. 2 LED light panels provide a
 763 diffused lighting. A circular cardboard wall of radius $R = 420$ mm delimited the border
 764 of experimental platform. The floor of the experimental platform was made with a rough
 765 wooden board that prevented the reflections of light. A computer is connected to the
 766 camera to supervise the actions of the robots in the arena, and to perform the necessary
 767 image processing to track each robot and compute in real time its position (x, y) and
 768 heading angle ϕ .

769 The clock cycle of the imaging process module is 300 ms, a limit imposed by the
 770 camera updating speed. A tracking software (Robots ID Tracker), based on the Kalman
 771 filter technology, is then used to assign the location data to the right robots on a shorter
 772 time scale (every 20 ms). These data are used in real time to control the reaction of
 773 each robot in its changing environment, and are also stored in the computer for off-line
 774 *a posteriori* trajectory analysis. Thanks to the high precision of our tracking system, we
 775 are able to compute in real time and for each robot i the quantities that characterize its
 776 instantaneous state with respect to its environment: the distance and relative orientation
 777 to the wall r_w^i and θ_w^i , and the distance, relative angular position, and relative orientation
 778 with respect to other robots j , d_{ij} , ψ_{ij} and ϕ_{ij} , respectively (Fig. 2). All this information
 779 is used to compute the output of the interactions of a robot with its local environment

780 by means of an Object-Oriented Programming software developed by us. The robot
 781 behavior is driven by the mathematical fish model, which combines the interactions with
 782 the obstacles and with the other robots, and generates the control signals dispatched
 783 in a distributed way to each individual robot through a WIFI communication router
 784 (HUAWEI WS831).

785 Although the robot has its own sensors to ensure it autonomous control and move-
 786 ments, in this work, we used a remote-control mode. This is because our goal was to
 787 compare the performances between the software simulation and the robot experiment
 788 with the same computational model and the same local information input (see the
 789 Hardware In Loop simulation in Fig. 13; [42]).

790 Fig. 13 (red and blue boxes) shows the “Hardware In Loop” (HIL) simulation used
 791 to control the Cuboids robots. The HIL simulation integrates the robots hardware into
 792 the distributed control loops of the platform computer software. As such, it differs
 793 from a traditional software simulation, being a semi-real one. Compared with pure
 794 theoretical simulations “in silico” (*i.e.*, the software simulation box in Fig. 13), the HIL
 795 simulation integrates both the hardware constraints (*i.e.*, the mechanical constraints of
 796 the robots, the time delay of the control loop which includes the shooting by the camera,
 797 the time of calculation and sending orders by the WIFI router), and those that result
 798 from the movement of the robots in a physical environment, in particular the need to
 799 avoid collisions with obstacles and other robots (see the blue box in Fig. 13).

800 The main difference between the HIL simulation and the software simulation is the
 801 real time control of the behavior of each robot, which is achieved by the *Motion Control*
 802 and the *Real Time Control* modules (see the red box in Fig. 13).

803 The Motion Control module can produce two kinds of motion patterns: rotating and
 804 moving straight. The first motion pattern is *Spot Rotation*, which means that the robot
 805 rotates around its center by means of wheels differential driving. The speed control of
 806 the two wheels is described by the following equation:

$$V_{R,i} = -V_{L,i} = p_t \delta\phi_{ci},$$

807 where $V_{R,i}$ and $V_{L,i}$ are the speeds of the right and left wheels of the robot respectively,
 808 p_t is a constant factor of proportionality, and $\delta\phi_{ci}$ is the real-time value of the heading
 809 variation, which is determined by the Real Time Control module. The second motion
 810 pattern that the robot can display is *Moving Straight*, where the speeds of the left and
 811 right wheels are the same:

$$V_{R,i} = V_{L,i} = p_m l_{ci},$$

812 where p_m is a constant factor of proportionality and l_{ci} is the value of the kick length,
 813 which is also determined by the Real Time Control module.

814 The Real Time Control module ensures the safe movement of each robot and helps
 815 the robot to rotate and move straight towards a target place. This module first converts
 816 the decision of the computational model ($\delta\phi_i(t_{dec}), l_i(t_{dec})$) at the last decision time t_{dec}
 817 into a real-time decision that is then performed by the robot, ($\delta\phi_{ci}(t), l_{ci}(t)$), $t > t_{dec}$.

818

820 **Algorithm of the Real Time Control module**

821

822 **Input :**

823 Computational Model decision: ($\delta\phi_i(t_{dec}), l_i(t_{dec})$),

824 Current position and heading: ($x_{ci}(t), y_{ci}(t)$), $\phi_{ci}(t)$.

825 **Output :**

826 Real-time decision: ($\delta\phi_{ci}(t_{dec}), l_{ci}(t_{dec})$)

```

827     1.  $\delta\phi_{ci}(t) = \phi_i(t_{dec}) + \delta\phi_i(t_{dec}) - \phi_{ci}(t), t > t_{dec}$ .
828     2.  $l_{ci}(t) = l_i(t_{dec}) - \sqrt{(x_{ci}(t) - x_i(t_{dec}))^2 + (y_{ci}(t) - y_i(t_{dec}))^2}$ .
829     3. If  $|\delta\phi_{ci}(t)| > \delta\phi_{Threshold}$ , then
830         Do Spot rotation for Motion Control in real-time.
831     else
832         Do Moving straight for Motion Control in real-time.
833     4. If  $|\delta\phi_{ci}(t)| < \delta\phi_{Threshold}$  and  $l_{ci}(t) < l_{Threshold}$ , then
834         the target is reached;
835         Goto Compute state (computational model) for a new decision.
836     5. If the path is not free, then
837         Do Obstacle Avoidance procedure.
838     6. End

```

841 There are two time-scales in the control for the robots. The long time scale is
842 determined by the time taken in simulating the computational model, which is about
843 1.3 s. The short time-scale corresponds to the Real Time Control module, which operates
844 at a high frequency with respect to the real time motion of the robot. This module is
845 used to control the navigation of the robot toward the target and the obstacle avoidance
846 (see the table of Algorithm of the Real Time Control module). The maximum time
847 interval of the Real Time Control module is 20 ms for each robot. With such a fast
848 frequency, the communication channel is always busy. To solve this problem, we designed
849 and used a specific protocol to broadcast in one loop the Motion Control command ($V_{R,i}$,
850 $V_{L,i}$) to each respective robot i , based on TCP protocol, thus guaranteeing the speed
851 and the robustness of the communication channel. The average duration of one of these
852 loops (for all robots) in the Real Time Control is about 13 ms (Fig. 13).

853 **Implementation of the behavioral model in the robots.** We use the LabVIEW
854 object-oriented programming (OOP) tool to design the distributed control software
855 for the Cuboids robots (Fig. 13). It first establishes independent memories for each
856 robot as an agent to store real time information, such as robot ID, location and heading
857 ($x_{ci}(t), y_{ci}(t), \phi_{ci}(t)$) at time t , and real time decision ($\delta\phi_{ci}(t), l_{ci}(t)$). We design a state
858 machine control structure to implement the HIL simulation control for each robot. With
859 the new speed control command determined by the *Motion Control* module, the actuators
860 of the robot are controlled wirelessly by the WIFI signals sent by the computer. The
861 robot controls its wheels to move towards the new target place while LED colors display
862 the state of the robot.

863 Robots use a constant kick length $l_i(t_{dec})$ of around 8 cm, that is, twice the body
864 length of a robot, which corresponds to the mean kick length measured in experiments
865 with five fish. Using a constant straight step also allows to check if the new target
866 place can be reached or not, in particular, to prevent the case where the agent could be
867 intercepted by another agent, in which case the distance traveled by the agent will be
868 shorter than $l_i(t_{dec})$.

869 The state machine control structure for an individual robot includes two main states:
870 COMPUTE state and MOVE state; see the flow chart of the robot state machine and
871 the finite state machine diagram in Fig. 14 and S8 Fig respectively. The robots are
872 programmed to perform a burst-and-coast movement mimicking the swimming mode of
873 fish. When a robot is in the COMPUTE state at time t_{dec} , the computational model
874 determines a new decision ($\delta\phi_i(t_{dec}), l_i(t_{dec})$) (see hereafter and [14] for the description

875 of the model; the model parameter for the robots are listed in 3 Table). After that, the
 876 robot switches to the MOVE state and adjusts its wheels to move towards the decision
 877 place in real time thanks to the *Motion Control* and *Real Time Control* modules. Since
 878 other robots are moving around asynchronously, the robot must avoid these dynamic
 879 obstacles while being in the MOVE state. To prevent collisions between robots, we
 880 designed and implemented an obstacle avoidance protocol. When no valid targets can
 881 be generated during the COMPUTE state (due to the impediment imposed by nearby
 882 robots), the robot generates a valid target place by means of a scanning method and,
 883 alternatively, just moves back over a short distance. However, this circumstance rarely
 884 occurs in our experiments (except in the absence of behavioral interactions, $k = 0$; see
 885 S5 Video).

886 We describe below the two states and the additional procedures used to avoid collisions
 887 with dynamical obstacles.

- 888 • COMPUTE State: This state generates a new decision $(\delta\phi_i(t_{dec}), l_i(t_{dec}))$ for
 889 the focal robot by means of the computational model, which is programmed in
 890 MATLAB. In this state, the robot takes the information about its local environment
 891 $(r_{w,i}, \theta_{w,i})$ and selects the neighbors to be taken into account corresponding to the
 892 current local interaction strategy. Then, the robot computes the variation of its
 893 heading angle $\delta\phi_i(t_{dec})$ that, combined with the kick length $l_i(t_{dec})$, determines a
 894 new target place. The location of the new target is then checked and validated
 895 by the OOP software so as to avoid any collision with static obstacles, before the
 896 robot switches to the MOVE state (see Fig. 14, S8 Fig). While a robot is in the
 897 COMPUTE State, the white LED light is turned on.
- 898 • MOVE State: In this state the robot evaluates whether its heading angle ϕ_{ci} is
 899 aligned with the new pace target. If the deviation $\delta\phi_{ci}$ is too large, the robot
 900 first rotates towards the target and then moves straight until it reaches the target,
 901 thanks to the *Motion Control* module. Then, when the robot successfully reaches
 902 the target, it returns to the COMPUTE state to determine a new target. While a
 903 robot is in the MOVE State, the green LED light is turned on.
- 904 • Obstacle Avoidance Protocol: This procedure is triggered as soon as the target
 905 path of the focal robot i crosses the safety zone of another robot j . The safety
 906 zone is a circular area around a robot of diameter of 80 mm. In this case, the
 907 focal robot i first stops and computes whether it can continue moving or not,
 908 according to the information it has about the distance d_{ij} and relative angular
 909 position ψ_{ij} of the neighboring robot. If the focal robot has the moving priority
 910 (determined by a large value of the angle of perception, $|\psi_{ij}| > 90^\circ$, meaning that
 911 the robot is a temporary leader [14]), or if the distance is larger than the diameter
 912 of the circle of security ($d_{ij} > 80$ mm, meaning that the robot j is far enough),
 913 the moving condition is satisfied and the focal robot i successfully switches back
 914 into the MOVE state. If not, it repeatedly checks the values d_{ij} and ψ_{ij} until the
 915 moving condition is satisfied. If the focal robot cannot go back into the MOVE
 916 state within 3 seconds, it toggles to the COMPUTE state to determine a new
 917 target.
- 918 • No Valid Target Procedure: This procedure is triggered when the robot is in the
 919 COMPUTE state and cannot generate a valid target place within 3 seconds. In
 920 this situation, the robot scans the local environment from its front to the nearest
 921 neighbor located at one of its sides. If there exists a free space for generating a
 922 target place, the robot toggles to the MOVE state. If, after scanning, no free space
 923 is available for moving, the robot moves back over a predefined distance of 80 mm
 924 (approximately two robot body lengths) and then toggles to the COMPUTE state
 925 to determine a new target place.

926 In the robotic experiments, we performed one experiment for each combination of
 927 interactions with about 8000 kicks in average for all the 5 robots. The duration time of
 928 experiments performed for each condition was the following:

- 929 • Interacting with $k = 1, 2$ and 3 nearest neighbors: 61, 62 and 63 min respectively.
- 930 • Interacting with $k = 1, 2$ and 3 randomly chosen neighbors: 65, 128 and 48 min
 931 respectively.
- 932 • Interacting with $k = 1$ and 2 most influential neighbors: 68 and 82 min respectively.
- 933 • Interacting with $k = 0$ and $k = 4$ neighbors: 150 min in both cases.

934 Data extraction and preprocessing

935 Fish data were extracted from videos recorded during 11 sessions along 11 days in 2013,
 936 by means of idTracker software version 2.1 [43], producing 11 data files with the position
 937 (in pixels) of each fish in each frame, with a time step of $\Delta t = 0.04$ s (corresponding
 938 to images taken with a frequency of 25 fps). Data were located in a rectangle of size
 939 $[471.23, 1478.48] \times [47.949, 1002.68]$ containing the circular tank of diameter 50 cm. The
 940 conversion factor from pixels to meters is 0.53×10^{-3} m/pix. The origin of coordinates
 941 $T(0, 0)$ is set to the center of the tank (Fig. 1).

942 We found that trajectory tracking was satisfactorily accurate. However, fish were
 943 often misidentified, making impossible the direct use of the data provided by the tracking
 944 system. We thus implemented a procedure of identity reassignment that provided us
 945 with the proper individual trajectories. In short, the procedure is a sorting algorithm
 946 where fish identities are successively reassigned in such a way that the coordinates of
 947 each fish at the next time step are the closest ones to the coordinates they had at the
 948 previous time. That is, the fish i at time t is assigned the coordinates of fish j at time
 949 $t + \Delta t$ that minimize the distance covered by the 5 fish.

950 Data were then grouped in a single file, counting 1.077.300 times, *i.e.*, almost 12 hours
 951 where the position of each fish is known. Then, times where at least one fish freezes
 952 were removed. Fish often remain stationary. We considered that a fish is at rest when
 953 the distance covered in 60 frames is smaller than 30 pixels, that is, when the mean speed
 954 is smaller than 6.6 mm/s during at least 2.4 seconds. We discarded more than half of
 955 the data using this procedure (around 5.5 hours of data remaining). We then extracted
 956 the continuous sequences lasting at least 20 seconds, obtaining 293 sequences for a total
 957 duration of around 3h 10mn.

958 Fish trajectories were then segmented according to the burst-and-coast typical
 959 behavior of this species [14] (see Fig. 1C). We used a time window of 0.2 s to find the
 960 local minima of the velocity. These points are used to define the onset of a kick event.
 961 We detected 60312 kicks, which means that a fish makes in average around 1 kick/s.

962 In [14], no statistically meaningful left/right asymmetry in the trajectories of single
 963 fish (~ 300000 kicks recorded) or pairs of fish (~ 200000 kicks recorded) was observed.
 964 Hence, for any observed trajectory, the mirror trajectory (that is the same one, but
 965 as observed from the bottom of the tank instead of from the top) would have exactly
 966 the same probability to be observed. Assuming the absence of left/right asymmetry for
 967 groups of 5 fish (as observed for 1 and 2 fish), leads to the same conclusion. Groups
 968 of 5 fish (as well as groups of 5 model fish or 5 robots) rotate clockwise (CW) or
 969 counter-clockwise (CCW) around the center of the tank for long periods (collective
 970 U-turns in groups of 2-20 fish have been studied in [36]). Therefore, for the much shorter
 971 present fish (and especially robots) experiments compared to [14] (60312 recorded kicks,
 972 instead of ~ 500000), one would observe an artificial asymmetry (groups turning more
 973 often CW than CCW, or the opposite) only due to the lack of statistical sampling of the

974 rare collective direction changes. In order to avoid this artificial asymmetry, for each
 975 set of 5 trajectories (fish and robots), we have added the mirror set (the trajectories
 976 as seen from the bottom of the tank). Again, this procedure is perfectly sound once
 977 the absence of left/right asymmetry observed in very long 1- and 2-fish experiments is
 978 reasonably assumed to hold in our present 5-fish experiments (the model and its version
 979 implemented in robots have obviously no left/right asymmetry, per construction). Note
 980 that only the distribution of θ_w^B is affected by this symmetrization procedure, and not
 981 the distributions of group cohesion, polarization, distance to the wall, counter-milling
 982 index (the latter being a relative quantity), which are invariant by the mirror symmetry.

983 To calculate the heading angle of a fish at time t , we considered that the direction
 984 of motion is well approximated by the velocity vector of the fish at that time t . The
 985 heading angle $\phi(t)$ of a fish is thus given by the angle that its velocity $\vec{v} = (v_x, v_y)$ makes
 986 with the horizontal line, that is,

$$\phi(t) = \text{ATAN2}(v_y(t), v_x(t)). \tag{1}$$

987 Positive angles are measured in counter-clockwise direction and ATAN2 returns a value in
 988 $(-\pi, \pi]$. The components of the velocity are estimated with backward finite differences,
 989 *i.e.*, $v_x(t) = (x(t) - x(t - \Delta t))/\Delta t$ and $v_y(t) = (y(t) - y(t - \Delta t))/\Delta t$.

990 The robot trajectories were extracted with a custom-made tracking software based
 991 on Kalman filter and pattern recognition technology [44]. Data were recorded every
 992 $\Delta t = 0.04$ s, and trajectories were then subjected to the same treatment.

993 Computational model

994 We use the same model to describe the time evolution of agents in the simulations and to
 995 control the decisions of the robots in the experiments, albeit with different parameters to
 996 accommodate for the different spatial and temporal scales in the two cases (see Table 3).

997 *Hemigrammus rhodostomus* displays a “burst-and-coast” swimming behavior char-
 998 acterized by sequences of sudden speed increases called “kicks”, each followed by a
 999 quasi-passive deceleration and gliding period along a near straight line until the next
 1000 kick (Fig. 1C, S1 Video, S3 Video).

1001 In our model, we consider that a fish makes the decision to change its heading and
 1002 to pick its new kick length and duration exactly at the onset of each kick [14]. The
 1003 behavior of an agent i is thus described by a sequence of kicking times t_i^n at which
 1004 the agent i performs its n -th kick. An agent selects a new heading depending on the
 1005 *instantaneous* state of its environment (other fish; obstacles), as perceived exactly at
 1006 the onset of a new kick, although the results of [28] suggest that the integration of
 1007 the necessary information by an actual fish can take a few tenths of a second during
 1008 the previous gliding period. Hence, at each of its kicking times t_i^n , the agent i collects
 1009 the information of its instantaneous relative position and heading with respect to the
 1010 obstacles and to the other agents, and selects the length and duration of its n -th kick, l_i^n
 1011 and τ_i^n respectively, and its change of direction, $\delta\phi_i^n$. Each agent has its own sequence
 1012 of kicking times, which are not necessarily equally spaced: $t_i^{n+1} - t_i^n \neq t_i^n - t_i^{n-1}$. In
 1013 addition, the motion of the different agents is asynchronous and their respective kicking
 1014 times are in general different. As the environment changes from one kick to another (the
 1015 agent moves with respect to the obstacles, and the other agents move with respect to
 1016 the agent), the quantities l_i^n , τ_i^n , and $\delta\phi_i^n$ are updated at each kicking time of agent i ,
 1017 according to the number and identity of the agents taken into account in the evaluation
 1018 of the effect of social interactions. In the present work, the number of agents taken into
 1019 account in the social interactions remains constant, while the identity of the neighbors
 1020 considered to interact with an agent is updated at each kicking time of this focal agent.

1021 The behavior of agent i (fish or robot) is thus described by the following discrete-time
 1022 decision model:

$$\vec{u}_i^{n+1} = \vec{u}_i^n + l_i^n \vec{e}(\phi_i^{n+1}), \quad (2)$$

$$\phi_i^{n+1} = \phi_i^n + \delta\phi_i^n, \quad (3)$$

1023 where \vec{u}_i^{n+1} and ϕ_i^{n+1} are the vector position and the heading of agent i at the end of its
 1024 n -th kick, and $\vec{e}(\phi_i^{n+1})$ is the unitary vector pointing in the direction of angle ϕ_i^{n+1} . At
 1025 the end of the n -th kick of agent i , the time is $t_i^{n+1} = t_i^n + \tau_i^n$, which is the next kicking
 1026 time of agent i . Note that one or more agents can perform one or more kicks between
 1027 two successive kicks of agent i . In that case, the kicking agent collects the information
 1028 about agent i (relative position and heading) to perform its own kick, while agent i is
 1029 simply in the gliding phase following its last kick.

1030 The kick length l_i^n is sampled at each kicking time of agent i from the bell-shaped
 1031 distribution of kick lengths obtained in our experiments of fish swimming in pairs [14],
 1032 whose mean value is $l = 7$ cm. When the new computed position of the agent would be
 1033 outside of the tank, a new kick length is sampled from the distribution. The typical
 1034 speed of fish right after a kick was found to be $v_0 \sim 14$ cm/s, and the speed was then
 1035 found to decay exponentially during the gliding phase, with a relaxation time $\tau_0 = 0.8$ s
 1036 (a feature implemented in the model in [14]). Thus, the duration of the time step τ_i^n ,
 1037 updated at each kicking time of agent i , is determined by the length of the kick and the
 1038 peak speed of the fish [14].

1039 The variation of the heading angle of agent i between two of its kicks is given by the
 1040 sum of the variations induced by its environment, that is,

$$\delta\phi_i^n = \delta\phi_{w,i}^n + \delta\phi_{R,i}^n + \sum_{\langle j,i \rangle} \delta\phi_{i,j}^n, \quad (4)$$

1041 where $\delta\phi_{w,i}^n$ is the angular variation caused by static obstacles (the wall of the fish tank
 1042 or the border of the robot platform), $\delta\phi_{R,i}^n$ is a random Gaussian white noise reflecting
 1043 the spontaneous fluctuations in the motion of the agent, and $\delta\phi_{i,j}^n$ is the angular variation
 1044 induced by the social interaction of the agent i with the agent j .

1045 The notation $\langle j, i \rangle$ indicates that the sum is performed over all the agents j considered
 1046 to interact with agent i . The number k of agents considered to interact with an agent
 1047 is part of what constitutes a social interaction strategy, and remains constant along
 1048 the whole simulation. When $k < N - 1$, the identity of these agents depends on the
 1049 strategy, but also on the instantaneous state of the system, so that their identity must
 1050 be updated at each kicking time of the focal agent i . At each kicking time t_i^n , the agents
 1051 are sorted according to the criterion used in the interaction strategy: the distance to the
 1052 focal agent $d_{ij}(t_i^n)$, a random selection of neighbors, or the influence on the focal agent
 1053 $\mathcal{I}_{ij}(t_i^n)$. Once sorted, the k first agents are considered in the sum in Eq. (4).

1054 Each contribution to the angle variation can be expressed in terms of decoupled
 1055 functions of the instantaneous state of the agents, that is, the distance and relative
 1056 orientation to the wall r_w and θ_w , and the distance d , viewing angle ψ , and relative
 1057 alignment ϕ between the focal fish and its considered neighbor (see Fig. 2A). The
 1058 derivation of these functions is based on physical principles of symmetry of the angular
 1059 functions and a sophisticated reconstruction procedure detailed in Calovi *et al.* [14] for
 1060 the case of *H. rhodostomus* and in [15] for the general case of animal groups.

1061 For completeness, we show these functions in S9 Fig and present here their analytical
 1062 expressions with the parameter values necessary to reproduce the simulations.

- 1063 • The repulsive effect of the wall is a centripetal force that depends only on the
 1064 distance to the wall r_w and the relative angle of the heading to the wall θ_w .

1065 Assuming that this dependence is decoupled, *i.e.*, $\delta\phi_w(r_w, \theta_w) = F_w(r_w) O_w(\theta_w)$,
 1066 we have:

$$F_w(r_w) = \gamma_w \exp \left[- \left(\frac{r_w}{l_w} \right)^2 \right], \quad O_w(\theta_w) = \beta_w \sin(\theta_w) \left(1 + 0.7 \cos(2\theta_w) \right), \quad (5)$$

1067 where $\gamma_w = 0.15$ is the intensity of the force ($F_w(0) = \gamma_w$), $l_w = 0.06$ m is the range
 1068 of the wall repulsion, and $\beta_w = 1.9157$ is a normalization constant of the angular
 1069 function $O_w(\theta_w)$, so that the mean of the squared function in $[-\pi, \pi]$ is equal to 1,
 1070 that is, $(1/2\pi) \int_{-\pi}^{\pi} O_w^2(\theta) d\theta = 1$. All angular functions are normalized in this way,
 1071 in order to allow the direct comparison of their shape in the different interactions.

1072 These parameter values are those used in the model simulations. They also appear
 1073 in Table 3, together with the values used in the experiments with robots.

- 1074 • The intensity of the stochastic spontaneous variation of heading $\delta\phi_R$ depends on
 1075 the distance to the wall r_w , and decreases as the fish gets closer to the wall and
 1076 becomes constrained by the boundary of the tank:

$$\delta\phi_R(r_w) = \gamma_R \left(1 - \alpha \exp \left[- \left(\frac{r_w}{l_w} \right)^2 \right] \right) g, \quad (6)$$

1077 where $\gamma_R = 0.45$, $\alpha = 2/3$, and g is a random number sampled from a standard
 1078 normal distribution (zero mean; unit variance). Random variations are minimal at
 1079 the border, where $r_w = 0$, $\delta\phi_R = \gamma_R(1 - \alpha)g$, and become larger as the individual
 1080 moves away from the border, *i.e.*, as r_w grows. Far from the border, the exponential
 1081 goes to zero and $\delta\phi_R = \gamma_R g$.

- 1082 • The interaction between agents can be decomposed into two terms of attraction
 1083 and alignment which depend only on the relative state of both interacting agents:

$$\delta\phi_{ij}(d_{ij}, \psi_{ij}, \phi_{ij}) = \delta\phi_{Att}^{ij} + \delta\phi_{Ali}^{ij}, \quad (7)$$

$$= \delta\phi_{Att}(d_{ij}, \psi_{ij}, \phi_{ij}) + \delta\phi_{Ali}(d_{ij}, \psi_{ij}, \phi_{ij}), \quad (8)$$

1084 where the relative state of fish j with respect to fish i is given by d_{ij} , the distance
 1085 between them; ψ_{ij} , the viewing angle with which fish i perceives fish j ; and
 1086 $\phi_{ij} = \phi_j - \phi_i$, the difference between their heading angle.

1087 We then define the *influence* $\mathcal{I}_{ij}(t)$ of a neighbor j on a focal individual i as the
 1088 absolute contribution of this neighbor to the instantaneous heading change of the
 1089 focal individual $\delta\phi_i(t)$ in Eq. (4), that is, for $j = 1, \dots, N$, $j \neq i$:

$$\mathcal{I}_{ij}(t) = |\delta\phi_{Att}^{ij}(t) + \delta\phi_{Ali}^{ij}(t)|. \quad (9)$$

1090 This precise definition is central to the implementation of the MOST INFLUENTIAL
 1091 interaction strategy involving the k most influential neighbors of a given focal fish i
 1092 (*i.e.*, the k neighbors with the largest influence $\mathcal{I}_{ij}(t)$)

1093 Following [14], we assume that both the attraction and the alignment functions
 1094 $\delta\phi_{Att}^{ij}$ and $\delta\phi_{Ali}^{ij}$ can be decomposed as the product of three functions that each
 1095 depend on only one of the three variables determining the relative state of the
 1096 two fish. Thus, for the attraction interaction, we have $\delta\phi_{Att}(d_{ij}, \psi_{ij}, \phi_{ij}) =$
 1097 $F_{Att}(d_{ij}) O_{Att}(\psi_{ij}) E_{Att}(\phi_{ij})$, where

$$F_{Att}(d) = \gamma_{Att} \left(\frac{d}{d_{Att}} - 1 \right) \frac{1}{1 + (d/l_{Att})^2}, \quad (10)$$

$$O_{Att}(\psi) = \beta_{Att} \sin(\psi) \left(1 - 0.33 \cos(\psi) \right), \quad (11)$$

$$E_{Att}(\phi) = \lambda_{Att} \left(1 - 0.48 \cos(\phi) - 0.31 \cos(2\phi) \right). \quad (12)$$

1098 Here, $d_{Att} = 3$ cm is the distance at which the short-range repulsion of individual
 1099 collision avoidance balances the long-range repulsion, $\gamma_{Att} = 0.12$ is the intensity
 1100 of the interaction, and $l_{Att} = 20$ cm characterizes the range where attraction is
 1101 maximum. The angular functions O_{Att} and E_{Att} are respectively normalized with
 1102 $\beta_{Att} = 1.395$ and $\lambda_{Att} = 0.9326$. As already mentioned when describing the
 1103 interaction with the wall, the three functional forms defined in (10–12) and the
 1104 numerical values of the coefficients have been extracted from experimental data by
 1105 means of a sophisticated procedure based on physical principles of symmetry of
 1106 the angular functions [14,15]. The names of the angular functions stand precisely
 1107 for their parity (Odd/Even).

1108 In the alignment, we have $\delta\phi_{Ali}(d_{ij}, \psi_{ij}, \phi_{ij}) = F_{Ali}(d_{ij}) E_{Ali}(\psi_{ij}) O_{Ali}(\phi_{ij})$, where

$$F_{Ali}(d) = \gamma_{Ali} \left(\frac{d}{d_{Ali}} + 1 \right) \exp \left[- \left(\frac{d}{l_{Ali}} \right)^2 \right], \quad (13)$$

$$E_{Ali}(\psi) = \beta_{Ali} \left(1 + 0.6 \cos(\psi) - 0.32 \cos(2\psi) \right), \quad (14)$$

$$O_{Ali}(\phi) = \lambda_{Ali} \sin(\phi) \left(1 + 0.3 \cos(2\phi) \right), \quad (15)$$

1109 with $d_{Ali} = 6$ cm, $l_{Ali} = 20$ cm, $\gamma_{Ali} = 0.09$, $\beta_{Ali} = 0.9012$, $\lambda_{Ali} = 1.6385$.

1110 The parameter values are those derived in [14] for the simulation model when fish
 1111 swim in pairs and are summarized in Table 3 (fish model and robots). More details
 1112 regarding the model, including the extraction of the above interaction functions, can be
 1113 found in [14].

1114 **Computational model in an unbounded domain.** Model simulations of agents
 1115 swimming in an unbounded domain were carried out by removing the interaction with
 1116 the wall (*i.e.*, by setting $\gamma_w = 0$; the rest of parameter values being those given in
 1117 Table 3).

1118 We have considered the MOST INFLUENTIAL and NEAREST interaction strategies, that
 1119 is, paying respectively attention to the k most influential neighbors or to the k -nearest
 1120 neighbors, for $k = 1, 2, 3$, and 4, and the case where agents do not interact with each
 1121 other ($k = 0$). Group cohesion and polarization are averaged over a large number of
 1122 simulation runs n : $\langle C(t) \rangle = (1/n) \sum_{i=1}^n C_i(t)$, where $C_i(t)$ is the group cohesion at time t
 1123 in the i -th run. We used $n = 1000$. The duration of each simulation was sufficiently
 1124 long to produce a total number of 10^4 kicks per run among the 5 agents (~ 2.7 hours).
 1125 A second series of simulations was carried out to produce 5×10^4 kicks (~ 13.5 hours),
 1126 finding the same qualitative results. Initial conditions of each run were always different,
 1127 with all agents located at less than $R = 25$ cm (the radius of the arena) from the origin
 1128 of coordinates.

1129 We first analyzed the impact on group cohesion and polarization (Fig. 9 and Fig. 10)
 1130 of reducing the attraction range in groups of $N = 5$ agents by truncating the attraction
 1131 intensity function F_{Att} when the neighbor is at a distance $d_{ij} > d_{cut}$ from the focal agent:
 1132 $F_{Att}(d_{ij}) = 0$, if $d_{ij} > d_{cut}$. For each value of d_{cut} , the mean cohesion was calculated as
 1133 the average over the last 10% of kicks over the 1000 runs carried out to obtain $\langle C(t) \rangle$, and
 1134 this, for both considered strategies and each value of k . When d_{cut} is sufficiently large,
 1135 the attraction range is sufficiently long and $\langle C(t) \rangle$ is close to the value corresponding to
 1136 the mean cohesion of the group when F_{Att} is not truncated. When d_{cut} is smaller than
 1137 a critical cut-off d_{cut}^* , the attraction range is too short and the agents simply diffuse,
 1138 with $\langle C(t) \rangle \sim t$ growing linearly in time Fig. 9.

1139 We then analyzed the group cohesion and polarization (Fig. 10 and S7 Fig) *i*) in
 1140 large groups of $N = 6, \dots, 70$ agents for the MOST INFLUENTIAL strategy with $k = 1$, *ii*)

1141 in a group of size $N = 20$, for different values of the number of nearest neighbors k with
 1142 which agents interact, and *iii*) in groups of size $N = 5, \dots, 26$, where agents interact with
 1143 their k nearest neighbors, for all the values of k between 1 and $N - 1$, except for $N = 22$,
 1144 24 and 26, where we limited the simulations to the interval of interest $k = 8, \dots, 12$. For
 1145 each combination of group size N and number of neighbors k considered, the number of
 1146 simulations, their duration, and the averaging procedure were the same as the ones used
 1147 in the analysis of the groups of size $N = 5$.

1148 Quantification of the collective behavior

1149 We characterize the collective behavioral patterns by means of five observables quantifying
 1150 the behavior of the group in the tank and the behavior of individuals inside the group. We
 1151 first write the coordinates of the position $\vec{u}_B = (x_B, y_B)$ and the velocity $\vec{v}_B = (v_x^B, v_y^B)$
 1152 of the barycenter B (center of mass) of the group with respect to the reference system
 1153 of the tank:

$$x_B(t) = \frac{1}{N} \sum_{i=1}^N x_i(t), \quad v_x^B(t) = \frac{1}{N} \sum_{i=1}^N v_x^i(t), \quad (16)$$

1154 with similar expressions for $y_B(t)$ and $v_y^B(t)$. The heading angle of the barycenter is
 1155 then given by $\phi_B = \text{ATAN2}(v_y^B, v_x^B)$.

1156 The barycenter defines a system of reference in which the relative position and velocity
 1157 of a fish, that we denote with a bar, are such that $\bar{x}_i = x_i - x_B$ and $\bar{v}_x^i = v_x^i - v_x^B$
 1158 (same expressions for the y -components). In the reference system of the barycenter, the
 1159 angle of the position of a fish is given by $\bar{\theta}_i = \text{ATAN2}(\bar{y}_i, \bar{x}_i)$, so the relative heading in
 1160 this reference system is $\bar{\phi}_i = \text{ATAN2}(\bar{v}_y^i, \bar{v}_x^i) \neq \phi_i - \phi_B$. We can thus define the angle of
 1161 incidence of a fish with respect to a circle centered at the barycenter as $\bar{\theta}_w^i = \bar{\phi}_i - \bar{\theta}_i$.
 1162 The angle $\bar{\theta}_w^i$ is the equivalent to the angle of incidence to the wall θ_w^i that we use in
 1163 the reference system of the tank, and serves to measure the angular velocity of a fish
 1164 with respect to the barycenter, in the reference system of the barycenter.

1165 The five observables used to quantify the behavior of a group are defined as follows:

- 1166 1. Group cohesion $C(t) \in [0, R]$:

$$C(t) = \sqrt{\frac{1}{N} \sum_{i=1}^N \|\vec{u}_i - \vec{u}_B\|^2}, \quad (17)$$

1167 where $\|\vec{u}_i - \vec{u}_B\|$ is the distance from fish i to the barycenter B of the N fish.

1168 Low values of $C(t)$ correspond to highly cohesive groups, while high values of $C(t)$
 1169 (in particular, comparable to the radius of the tank) imply that individuals are
 1170 spatially dispersed.

- 1171 2. Group polarization $P(t) \in [0, 1]$:

$$P(t) = \frac{1}{N} \left\| \sum_{i=1}^N \vec{e}_i(t) \right\|, \quad (18)$$

1172 where $\vec{e}_i = \vec{v}_i / \|\vec{v}_i\| = (\cos(\phi_i), \sin(\phi_i))$ is the unit vector in the direction of motion
 1173 of the individual fish, given by its velocity vector \vec{v}_i .

1174 A value of P close to 1 would mean that the N individual headings are aligned
 1175 and point in the same direction, while a value of P close to 0 would mean that the
 1176 N vectors point in different directions, but can also mean that vectors are collinear

1177 and with opposite direction (*e.g.*, for N even, half of the vectors point North, the
 1178 other half point South) so that they cancel each other. Similarly, when $N = 5$ and
 1179 two normalized velocity vectors cancel each other (*e.g.*, when 4 fish swim in the
 1180 same direction \vec{e} and one fish swims in the opposite direction $-\vec{e}$) would give rise
 1181 to a resultant vector of norm $P = (4 \times 1 - 1)/5 = 3/5 = 0.6$, and if two pairs of
 1182 fish cancel each other, then $P = (3 \times 1 - 2 \times (-1))/5 = 1/5 = 0.2$.

1183 Note that uncorrelated headings would lead to $P \sim 1/\sqrt{N}$, which becomes small
 1184 only for large group size N , but which is markedly lower than 1 for any $N \geq 5$.

1185 3. Distance of the barycenter to the wall $r_w^B(t) \in [0, R]$:

$$r_w^B(t) = R - \sqrt{(x_B(t))^2 + (y_B(t))^2}, \quad (19)$$

1186 Note that when the individuals move in a cohesive group, r_w^B is typically of the
 1187 same order as the mean distance of agents to the wall $\langle r_w \rangle = (1/N) \sum_{i=1}^N r_w^i$.
 1188 When the group is not cohesive, r_w^B is of order of the radius of the tank.

1189 4. Relative angle of the barycenter heading to the wall $\theta_w^B(t) \in [-\pi, \pi]$:

$$\theta_w^B(t) = \text{ATAN2}(v_y^B(t), v_x^B(t)). \quad (20)$$

1190 When the group swims along the wall $\theta_w^B(t) \approx \pm\pi/2$ (*i.e.*, $\theta_w^B(t) \approx \pm 90^\circ$).

1191 5. Index of collective counter-milling and super-milling $Q(t) \in [-1, 1]$:

$$Q(t) = \left(\frac{1}{N} \sum_{i=1}^N \sin(\theta_w^i(t)) \right) \times \text{SIGN} \left(\frac{1}{N} \sum_{i=1}^N \sin(\theta_w^i(t)) \right) \quad (21)$$

$$= \Gamma_B(t) \times \text{SIGN}(\Gamma(t)). \quad (22)$$

1192 A group of fish rotating around the center of the tank with a rotation index $\Gamma(t)$
 1193 (defined in Eq. (22); similar to an angular momentum) would display a counter-
 1194 milling behavior if the individual fish also rotate around the barycenter of the group
 1195 and both directions of rotation are opposite. The first sum between parentheses
 1196 in Eq. (21) is the index of rotation of the fish with respect to the barycenter of
 1197 the group, denoted by $\Gamma_B(t)$ in Eq. (22). Multiplying by the sign of $\Gamma(t)$ means
 1198 that when $Q(t) < 0$, both directions are opposite and the fish exhibit a *collective*
 1199 *counter-milling behavior*, while when $Q(t) > 0$, both rotations are in the same
 1200 direction and the fish exhibit a *collective super-milling behavior*.

1201 Thus, a group of 5 individuals turning around the center of the tank in a rigid
 1202 formation that always points North, like the fingertips of the hand when cleaning
 1203 a window, would correspond to a perfect counter-milling behavior. On the other
 1204 hand, a situation where individuals rotate around the center of the tank as if they
 1205 were fixed to a vinyl record, so that trajectories are perfect circles and individuals
 1206 far from the center of the tank move faster than those close to the center, would
 1207 correspond to a zero-milling state. Actual groups of fish present an intermediate
 1208 behavior between these two situations, with a clear bias towards negative values of
 1209 $Q(t)$ (see Fig. 3 for fish, S4 Video for robots, and Fig. 8 for fish, model fish, and
 1210 robots).

1211 Collective behavior is thus quantified by means of the probability density functions
 1212 of these quantities. In addition, density maps are presented in order to illustrate the
 1213 correlations between the polarization P and the group cohesion C in fish experiments,

1214 model simulations, and robot experiments (S1 Fig–S4 Fig). We consider two normaliza-
 1215 tions: *i*) with the total number of data, to highlight the significant regions of the map
 1216 and neglect the regions where the data are scarce (S1 Fig for the fish model, and S3
 1217 Fig for robot experiments); *ii*) with the total number of data in a given range of the
 1218 polarization, so that each row in the map is a PDF of C for a given P (S2 Fig for the
 1219 fish model, and S4 Fig for robot experiments). Spatial distances in the model and robot
 1220 experiments are rescaled with the respective scaling factor $\lambda_M = 0.87$ and $\lambda_R = 0.35$ to
 1221 allow for a direct comparison of our two spatial quantifiers (C and r_w^B) with the results
 1222 of fish experiments (the three other quantifiers P , θ_w^B , and Q are not affected by this
 1223 rescaling).

1224 Quantifier for the similarity of probability distribution functions

1225 In the Results section, we qualitatively compare the probability distribution functions
 1226 (PDF) of the group cohesion, polarization, distance to the wall, angle with respect to
 1227 the wall, and counter-milling index featured in Figs. 4–8, for the 3 interaction strategies
 1228 (NEAREST; RANDOM; MOST INFLUENTIAL), and for $k = 1, 2, 3$ interacting neighbors (as
 1229 well as the cases $k = 0$ – no interaction – and $k = 4$).

1230 Here, we consider the Hellinger distance $D(F|G)$ [45,46] to precisely quantify the
 1231 “similarity” of two PDF $F(x)$ and $G(x)$ for the same observable x (one of the 5 listed
 1232 above that we have considered):

$$D(F|G) = \frac{1}{2} \int \left(\sqrt{F(x)} - \sqrt{G(x)} \right)^2 dx = 1 - \int \sqrt{F(x)} \sqrt{G(x)} dx, \quad (23)$$

1233 where we have used the normalization of the PDF, $\int F(x) dx = \int G(x) dx = 1$, to
 1234 obtain the last equality. The first definition of $D(F|G)$ makes clear that it measures the
 1235 overall difference between $F(x)$ and $G(x)$, while the second equivalent definition has a
 1236 nice interpretation in terms of the *overlap* of both PDF. Indeed, the second definition
 1237 measures the distance from unity of the scalar product of $\sqrt{F(x)}$ and $\sqrt{G(x)}$ seen as
 1238 vectors of unit Euclidean norm (a consequence of the normalization, $\int \sqrt{F(x)}^2 dx = 1$).

1239 The Hellinger distance is zero if and only if $F(x) = G(x)$, and it always satisfies
 1240 $D(F|G) \leq 1$. The upper bound $D(F|G) = 1$ is reached whenever the supports of the
 1241 two PDF are not intersecting, so that $F(x) \times G(x) = 0$, for all values of x . In practice,
 1242 a value of $D(F|G) \geq 0.1$ points to the two PDF being markedly dissimilar.

1243 Of course, using the Hellinger distance is an arbitrary choice and other distances
 1244 (like the Kolmogorov-Smirnov distance) could lead to slightly different relative dis-
 1245 tances/errors, but would not change our conclusions when the PDF are markedly
 1246 different. In particular, the fact that the MOST INFLUENTIAL strategy is the strategy for
 1247 $k = 1$ leading to the best agreement with fish experiments would be recovered by any
 1248 meaningful quantifier.

1249 We have computed the Hellinger distance between PDF measured in fish experiments
 1250 and the corresponding PDF measured in the fish model simulations (Table 1) and
 1251 in robots experiments (Table 2), hence providing a more precise, albeit not unique,
 1252 quantification of their similarity.

1253 Acknowledgments

1254 We thank the three anonymous referees for their thoughtful comments on the manuscript.
 1255 We are grateful to Patrick Arrufat and Gérard Latil for technical assistance.

1256 **References**

- 1257 1. D. J. T. Sumpter (2010) *Collective Animal Behavior*. Princeton, NJ: Princeton
1258 University Press.
- 1259 2. I. D. Couzin (2002) Collective cognition in animal groups. *Trends in Cognitive
1260 Science*, 13(1):36433.
- 1261 3. M. Moussaïd, S. Garnier, G. Theraulaz and D. Helbing (2009) Collective infor-
1262 mation processing in swarms, flocks and crowds. *Topics in Cognitive Science* 1,
1263 469–497.
- 1264 4. S. Camazine, J. L. Deneubourg, N. Franks, J. Sneyd, G. Theraulaz and
1265 E. Bonabeau (2001) *Self-Organization in Biological Systems*. Princeton, NJ: Prince-
1266 ton University Press.
- 1267 5. I. D. Couzin and J. Krause (2003) Self-organization and collective behavior in
1268 vertebrates. *Advances in the Study of Behavior* 32: 1–75.
- 1269 6. U. Lopez, J. Gautrais, I. D. Couzin and G. Theraulaz (2012) From behavioural
1270 analyses to models of collective motion in fish schools. *Interface Focus* 2:693–707.
- 1271 7. A. Cavagna, A. Cimarelli, I. Giardina, G. Parisi, R. Santagati, F. Stefanini and
1272 R. Tavarone (2010) From empirical data to inter-individual interactions: unveiling
1273 the rules of collective animal behavior. *Mathematical Models and Methods in
1274 Applied Sciences* 20:1491–1510.
- 1275 8. D. J. T. Sumpter (2006) The principles of collective animal behaviour. *Philoso-
1276 phical Transactions of the Royal Society B: Biological Sciences* 361 (1465):5–22.
- 1277 9. T. Sasaki and S. C. Pratt (2018) The Psychology of Superorganisms: Collective
1278 Decision Making by Insect Societies. *Annual Review of Entomology* 63:259–275.
- 1279 10. C. Detrain and J. L. Deneubourg (2006) Self-organized structures in a superorgan-
1280 ism: Do ants “behave” like molecules? *Physics of Life Reviews* 3(3):162–187.
- 1281 11. C. Detrain and J. L. Deneubourg (2008) Collective decision-making and foraging
1282 patterns in ants and honeybees. *Advances in Insect Physiology* 35:123–173.
- 1283 12. T. D. Seeley (1996) *Wisdom of the Hive*. Cambridge, MA: Harvard Univ. Press.
- 1284 13. T. D. Seeley (2010) *Honeybee Democracy*. Princeton, NJ: Princeton Univ. Press.
- 1285 14. D. S. Calovi, A. Litchinko, V. Lecheval, U. Lopez, A. Pérez Escudero, H. Chaté,
1286 C. Sire, G. Theraulaz (2018) Disentangling and modeling interactions in fish with
1287 burst-and-coast swimming reveal distinct alignment and attraction behaviors.
1288 *PLoS Comput. Biol.* 14(1):e1005933.
- 1289 15. R. Escobedo, V. Lecheval, V. Papaspyros, F. Bonnet, F. Mondada, C. Sire, and
1290 G. Theraulaz (2019). A data-driven method for reconstructing and modelling
1291 social interactions in animal groups. <https://doi.org/10.1101/816777>.
- 1292 16. J. K. Parrish, S. V. Viscido and D. Grunbaum (2002) Self-organized fish schools:
1293 An examination of emergent properties. *Biological Bulletin* 202:296–305.
- 1294 17. T. Vicsek and A. Zafeiris (2012) Collective motion. *Physics Reports* 517: 71–14.
- 1295 18. I. Aoki (1982) A simulation study on the schooling mechanism in fish. *Bull. J.
1296 Soc. Sci. Fish* 48(8):1081–1088.

- 1297 19. I. D. Couzin, J. Krause, R. James, G. Ruxton and N. Franks (2002) Collective
1298 memory and spatial sorting in animal groups. J. Theor. Biol. 218(5):1–11.
- 1299 20. T. Vicsek, A. Cziřok, E. Ben-Jacob, I. Cohen and O. Shochet (1995) Novel type
1300 of phase transition in a system of self-driven particles. Physical Review Letters
1301 75: 226–1229.
- 1302 21. M. Ballerini et al.(2008) Interaction ruling animal collective behavior depends on
1303 topological rather than metric distance: Evidence from a Field Study. Proc. Natl.
1304 Acad. Sci. USA 105:1232–1237.
- 1305 22. M. Camperi, A. Cavagna, I. Giardina, G. Parisi and E. Silvestri (2012) Spa-
1306 tially balanced topological interaction grants optimal cohesion in flocking models.
1307 Interface Focus 2:715–725.
- 1308 23. J. Gautrais *et al.* (2012) Deciphering interactions in moving animal groups. PLoS
1309 Comp. Biol. 8(9):e1002678.
- 1310 24. S. B. Rosenthal, C. R. Twomey, A. T. Hartnett, H. S. Wu, and I. D. Couzin (2015)
1311 Revealing the hidden networks of interaction in mobile animal groups allows
1312 prediction of complex behavioral contagion. Proc. Natl. Acad. Sci. USA 112
1313 15):4690–4695.
- 1314 25. B. H. Lemasson, J.. J. Anderson and R.A. Goodwin (2009) Collective motion
1315 in animal groups from a neurobiological perspective: the adaptive benefits of
1316 dynamic sensory loads and selective attention. Journal of Theoretical Biology
1317 261(4):501–510.
- 1318 26. B.. H. Lemasson, J.. J. Anderson and R.A. Goodwin (2013) Motion-guided atten-
1319 tion promotes adaptive communication during social navigation. Proceedings of
1320 the Royal Society of London B: Biological Sciences 280(1754):20122003.
- 1321 27. A. M. Calvao and E. Brigatti (2014) The role of neighbours selection on cohesion
1322 and order of swarms. PLoS ONE 9(5): e94221.
- 1323 28. L. Jiang, L. Giuggioli, A. Perna, R. Escobedo, V. Lecheval, C. Sire, Z. Han, and
1324 G. Theraulaz (2017) Identifying influential neighbors in animal flocking. PLoS
1325 Comput. Biol. 13:e1005822.
- 1326 29. Y. Katz, K. Tunstrøm, C. Ioannou, C. Huepe, and I. D. Couzin (2011) Inferring
1327 the structure and dynamics of interactions in schooling fish. Proc. Natl. Acad.
1328 Sci. USA 108(46):18720–18725.
- 1329 30. A. E. Turgut, H. Çelikkanat, F. Gökçe, and E. Şahin (2008) Self-organized flocking
1330 in mobile robot swarms. Swarm Intelligence 2:97–120.
- 1331 31. C. Muro, R. Escobedo, L. Spector, and R. P. Coppinger (2011) Wolf-pack (*Canis*
1332 *lupus*) hunting strategies emerge from simple rules in computational simulations.
1333 Behav. Processes 88(3):192–197.
- 1334 32. D. S. Calovi, U. Lopez, S. Ngo, C. Sire, H. Chaté, and G. Theraulaz (2014)
1335 Swarming, Schooling, Milling: Phase diagram of a data-driven fish school model.
1336 New J. Phys., 16:015026.
- 1337 33. R. Dukas (2002) Behavioural and ecological consequences of limited attention.
1338 Phil. Trans. R. Soc. Lond. B 357:1539–1547.

- 1339 34. Nagy M., Akos Z., Biro D., and Vicsek T. (2010) Hierarchical group dynamics in
1340 pigeon flocks. Nature 464:890–893.
- 1341 35. Herbert-Read J. E., Perna A., Mann R. P., Schaerf, T. M., Sumpter D. J., and
1342 Ward A. J. (2011) Inferring the rules of interaction of shoaling fish. Proc. Natl.
1343 Acad. Sci. USA 108(46):18726–18731.
- 1344 36. V. Lecheval, L. Jiang., P. Tichit, C. Sire, C. K. Hemelrijk, and G. Theraulaz (2018)
1345 Social conformity and propagation of information in collective U-turns of fish
1346 schools. Proc. Roy. Soc. B, 285:20180251.
- 1347 37. A. Huth and C. Wissel (1992). The simulation of the movement of fish schools. J.
1348 Theor. Biol. 156(3):365–385.
- 1349 38. H. S. Niwa (1994). Self-organizing dynamic model of fish schooling. J. Theor. Biol.
1350 171(2):123–136.
- 1351 39. N. W. Bode, D. W. Franks, and A. J. Wood (2010). Limited interactions in flocks:
1352 relating model simulations to empirical data. J. R. Soc. Interface 8:301–304.
- 1353 40. E. I. Knudsen (2018) Neural Circuits That Mediate Selective Attention: A Com-
1354 parative Perspective. Trends in Neurosciences, 41:789–805.
- 1355 41. C. Reynolds (1987) Flocks, herds and schools: A distributed behavioral model.
1356 Computer Graphics 21(4) (SIGGRAPH '87 Conference Proceedings), pp. 25–34.
- 1357 42. X. Hu (2005) Applying robot-in-the-loop-simulation to mobile robot systems. In
1358 Advanced Robotics, 2005. ICAR'05 Proceedings, 12th International Conference
1359 on, p. 506–513.
- 1360 43. A. Pérez-Escudero, J. Vicente-Page, R. C. Hinz, S. Arganda, and G. G. de Polavieja
1361 (2014) idTracker: tracking individuals in a group by automatic identification of
1362 unmarked animals. Nature Methods 11:743–748.
- 1363 44. J. Goncalves, J. Lima, and P. Costa (2008) Real-time localization of an omni-
1364 directional mobile robot resorting to odometry and global vision data fusion:
1365 An EKF approach. IEEE International Symposium on Industrial Electronics, pp.
1366 1275–1280.
- 1367 45. A. Basu, I. R. Harris, S. Basu (1997). Minimum distance estimation: the approach
1368 using density based distances. In: G. S. Maddala, C. R. Rao (Eds.), Handbook of
1369 Statistics, Vol. 15, Robust Inference. Elsevier Science, New York, NY, pp. 21–48.
- 1370 46. R. Beran (1977). Minimum Hellinger distance estimates for parametric models.
1371 Annals of Statistics 5:445–463.

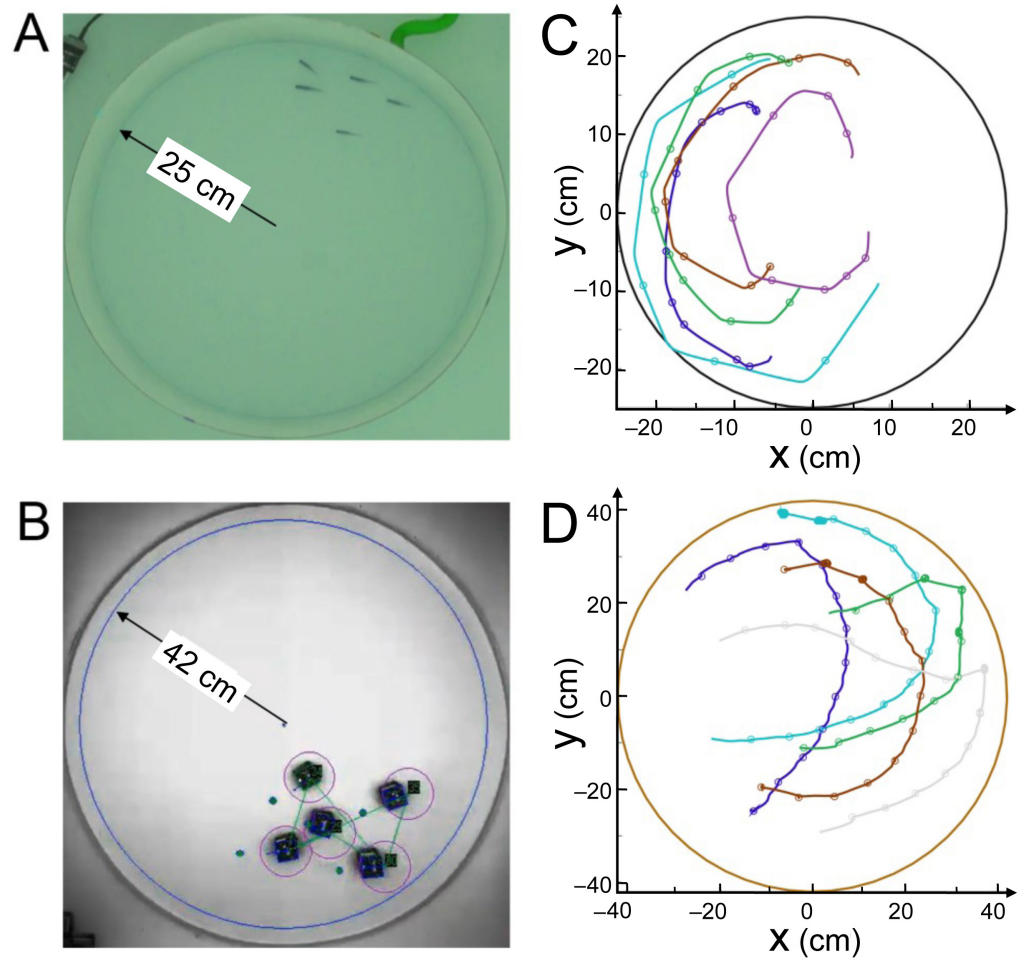


Fig 1. Experimental setups and tracking. (A) Experiments with 5 fish swimming in a tank of radius $R_{\text{fish}} = 25$ cm. (B) 5 robots running in a platform of radius $R_{\text{robot}} = 42$ cm. (C) Individual fish trajectories over 4 seconds. The circles represent the onset of bursts, when speed is minimum. (D) Individual trajectories in one robotic experiment over 24 seconds. The circles indicate the decisions of the robots to select a new target place, when individual speed is minimum.

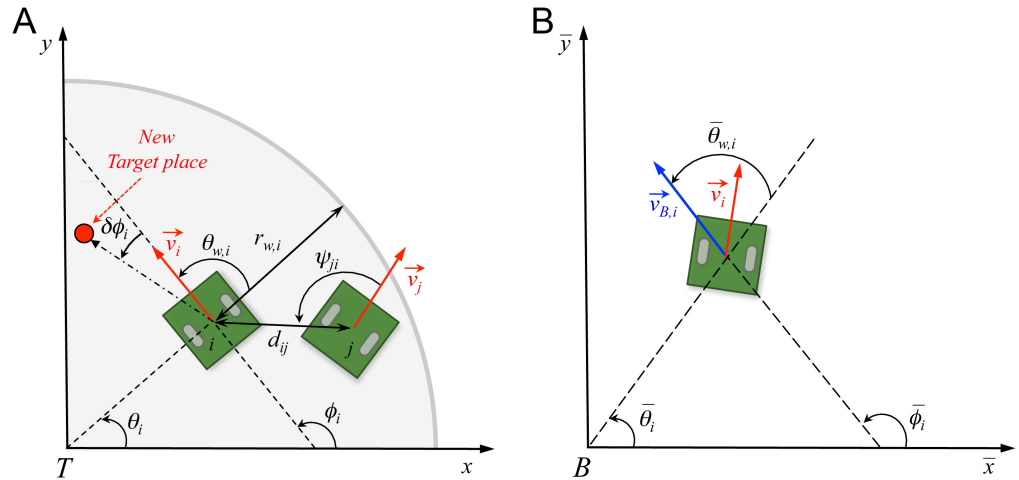


Fig 2. Angles and reference systems. (A) Distances, angles, and velocity vectors of agents i and j in the absolute reference system centered in $T(0,0)$. Positive values of angles are fixed in the anticlockwise direction. θ_i is the position angle of agent i with respect to T and the horizontal line; $r_{w,i}$ is the distance of agent i from the nearest wall; ϕ_i is the heading angle of agent i , determined by its velocity vector \vec{v}_i ; $\theta_{w,i}$ is the relative angle of agent i with the wall; d_{ij} is the distance between agents i and j ; ψ_{ij} is the viewing angle with which agent i perceives agent j , *i.e.*, the angle between the velocity of i and the vector $\vec{i}j$ (we show the angle $\psi_{ji} \neq \psi_{ij}$ with which j perceives i , for the sake of readability of the figure); $\phi_{ij} = \phi_j - \phi_i$ is the difference of heading between agents i and j , and $\delta\phi_i$ is the variation of heading of agent i . (B) Relative reference system centered in the barycenter of the group $B(x_B, y_B)$. Relative variables are denoted with a bar. Angle $\bar{\theta}_{w,i} = \bar{\phi}_i - \bar{\theta}_i$ is the angle of incidence of the relative speed of agent i with respect to a circle centered in B .

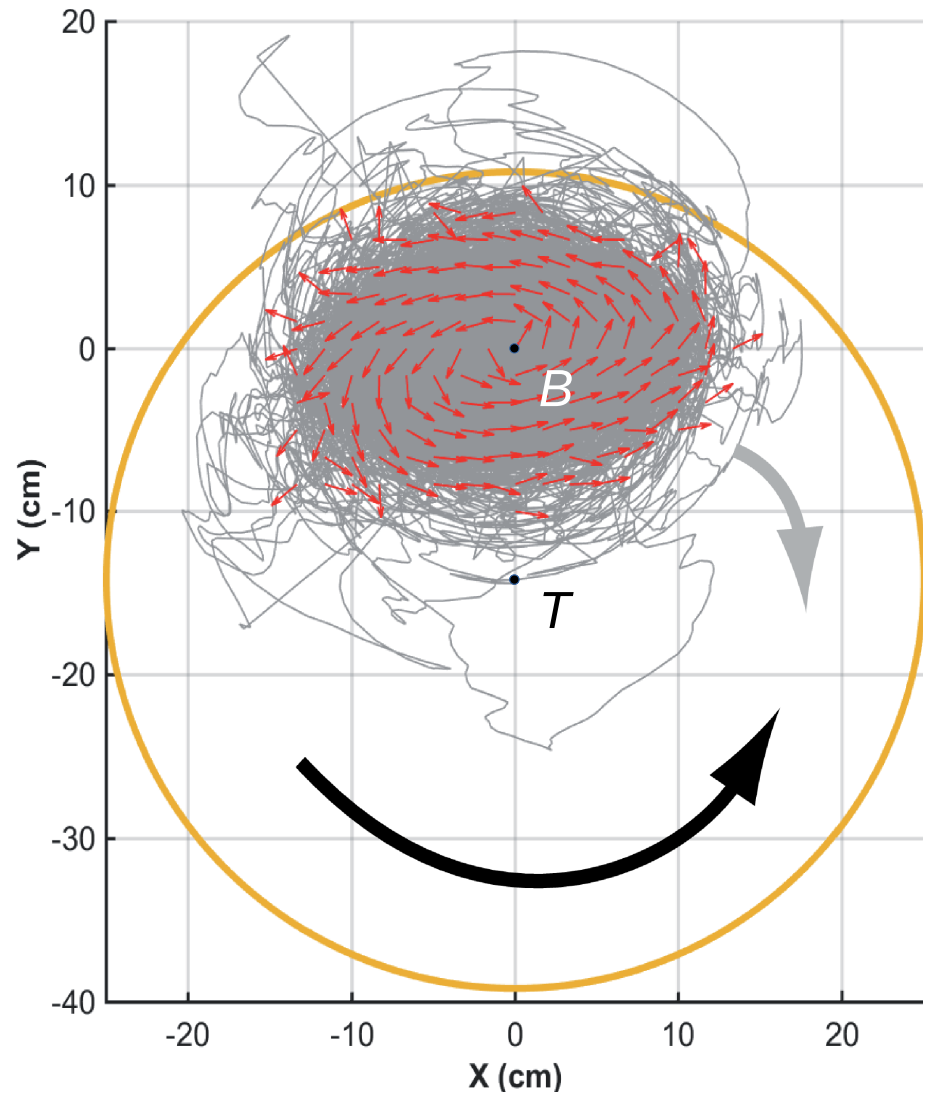


Fig 3. Counter-milling in fish experiments. Individual fish (small red arrows) turn counter-clockwise (CCW) around their barycenter, here located at $B(0,0)$, while the fish group rotates clockwise (CW) around the center of the tank, located at $T(0,-14)$ in the reference system of the barycenter. Red arrows (of same length) denote relative fish heading, gray lines denote relative trajectories, and large orange circle denotes the average relative position of the border of the tank. The wide black arrow shows the direction of rotation of individual fish with respect to B (CCW), opposite to the wide gray arrow showing the direction of rotation of the group with respect to T (CW).

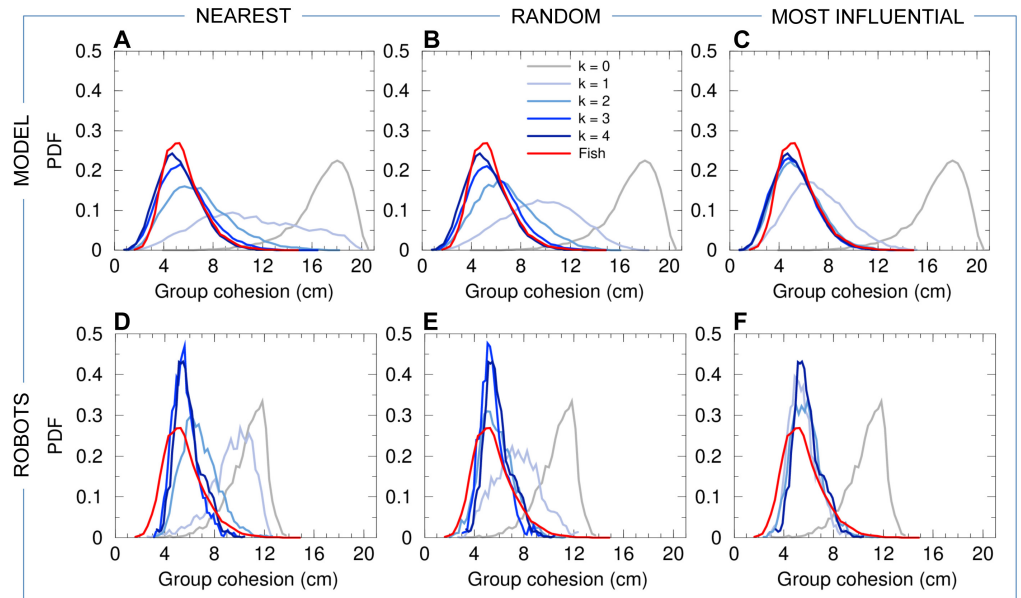


Fig 4. Group cohesion. Probability density functions (PDF) of the group cohesion C for the experiments with 5 fish (red line in all panels), model simulations (panels ABC), and experiments with 5 robots (panels DEF), compared to the corresponding null models ($k = 0$, no interaction between individuals) in both simulations and robots (gray line in all panels). Distances have been rescaled by $\lambda_M = 0.87$ for the model simulations, and by $\lambda_R = 0.35$ for the robot experiments. The intensity of blue is proportional to the number of neighbors interacting with a focal individual (agent or robot), from $k = 1$ (light blue) to $k = 4$ (dark blue). Interaction strategies involve the k NEAREST neighbors (panels AD), k RANDOM neighbors (panels BE), and the k MOST INFLUENTIAL neighbors (panels CF).

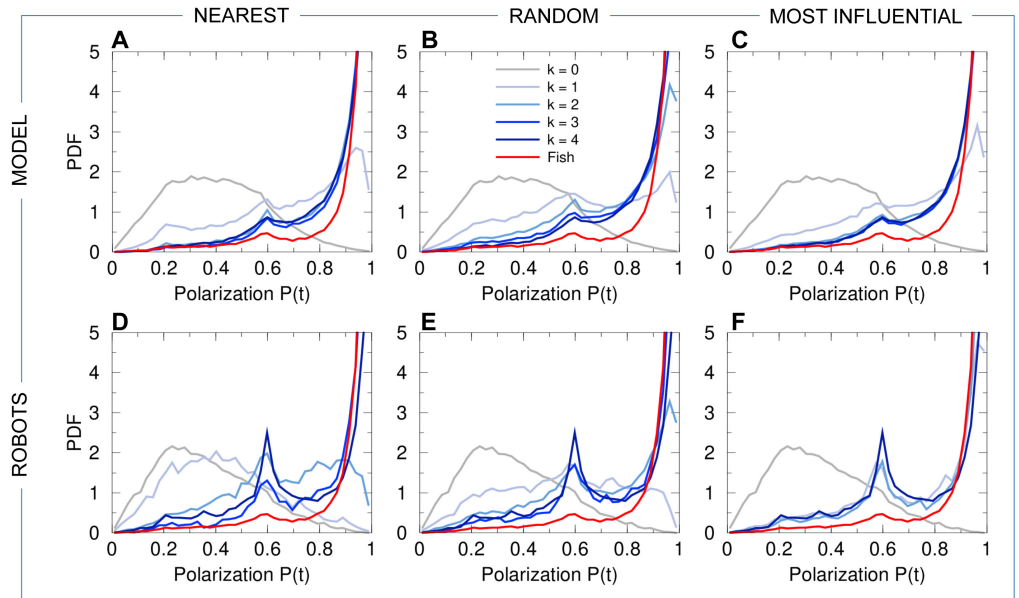


Fig 5. Group polarization. PDF of the group polarization P for fish experiments (red line in all panels), model simulations (panels ABC), and robot experiments (panels DEF), compared to the corresponding null models ($k = 0$, no interaction between individuals) in both simulations and robots (gray line in all panels). Curves for agents (fish model and robots) are in blue and gray, depending on the value of k (see legend in panel B). Interaction strategies involve the k NEAREST neighbors (panels AD), k RANDOM neighbors (panels BE), and the k MOST INFLUENTIAL neighbors (panels CF).

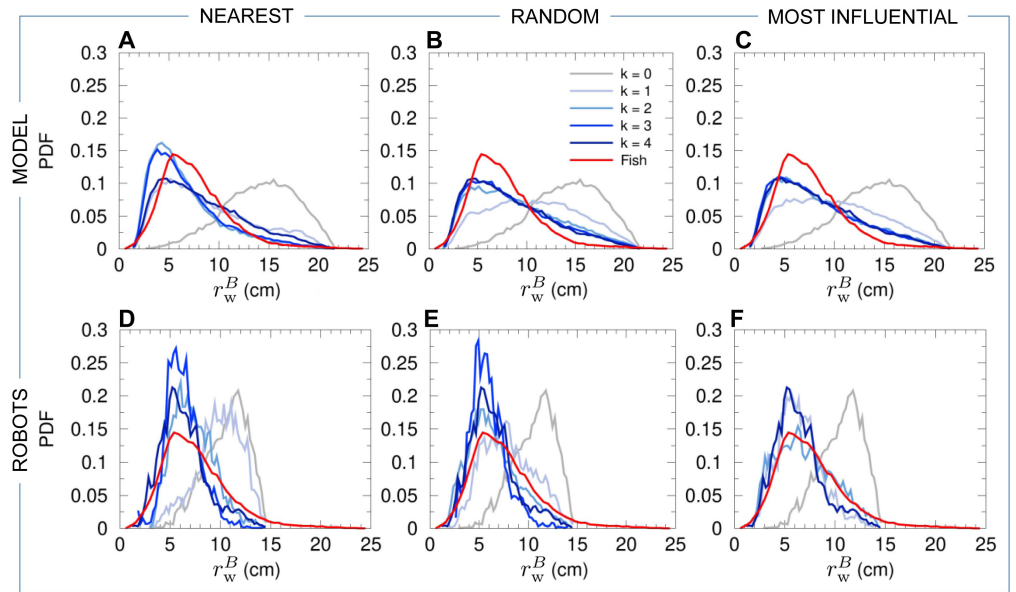


Fig 6. Distance of the barycenter of the individuals to the wall. PDF of the distance r_w^B of the barycenter of the individuals from the wall for fish experiments (red line in all panels), model simulations (panels ABC), and robot experiments (panels DEF), compared to the corresponding null models ($k = 0$, no interaction between individuals) in both simulations and robots (gray line in all panels). Distances have been rescaled by $\lambda_M = 0.87$ for the model simulations, and by $\lambda_R = 0.35$ for the robot experiments. Curves for agents (fish model and robots) are in blue and gray, depending on the value of k (see legend in panel B). Interaction strategies involve the k NEAREST neighbors (panels AD), k RANDOM neighbors (panels BE), and the k MOST INFLUENTIAL neighbors (panels CF).

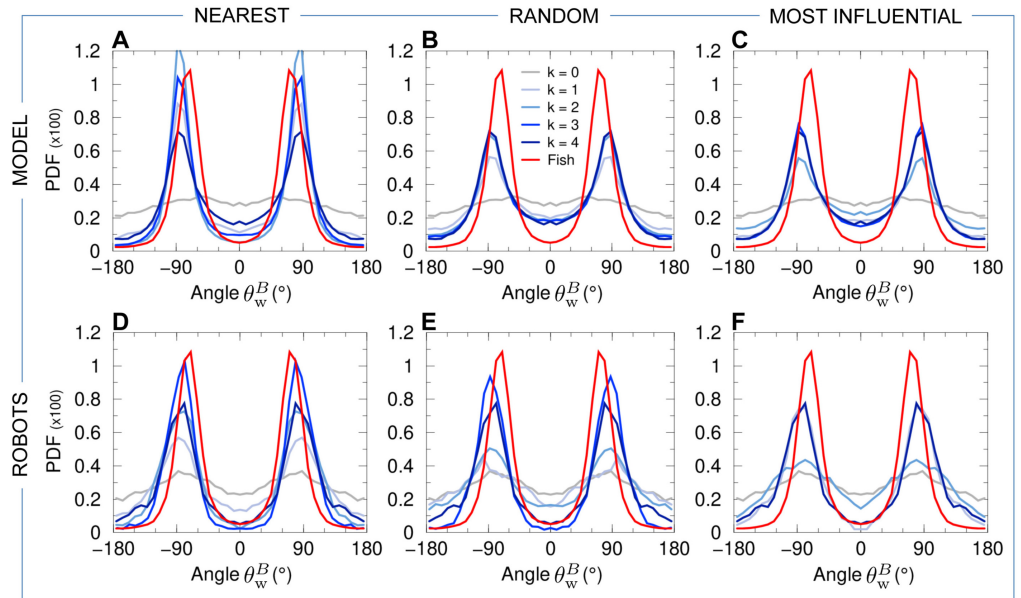


Fig 7. Relative angle of the heading of the barycenter of the group with the wall. PDF of the relative angle θ_w^B of the heading of the barycenter of the group with the wall for fish experiments (red line in all panels), model simulations (panels ABC), and robot experiments (panels DEF), compared to the corresponding null models ($k = 0$, no interaction between individuals) in both simulations and robots (gray line in all panels). Curves for agents (fish model and robots) are in blue and gray, depending on the value of k (see legend in panel B). Interaction strategies involve the k NEAREST neighbors (panels AD), k RANDOM neighbors (panels BE), and the k MOST INFLUENTIAL neighbors (panels CF).

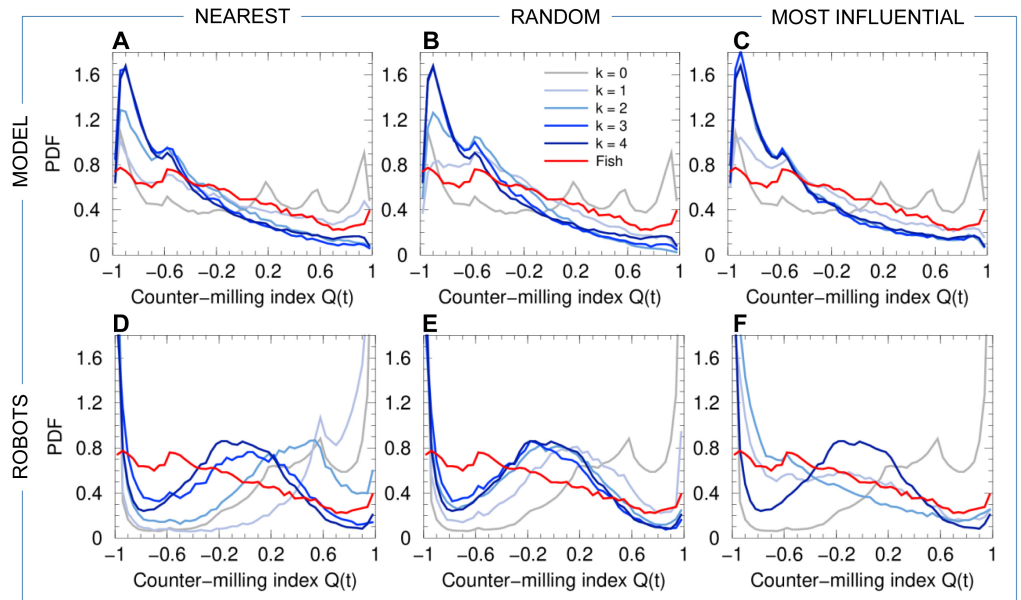


Fig 8. Counter-milling index. PDF of the counter-milling index Q for fish experiments (red line in all panels), model simulations (panels ABC), and robot experiments (panels DEF), compared to the corresponding null models ($k = 0$, no interaction between individuals) in both simulations and robots (gray line in all panels). Curves for agents (fish model and robots) are in blue and gray, depending on the value of k (see legend in panel B). Interaction strategies involve the k NEAREST neighbors (panels AD), k RANDOM neighbors (panels BE), and the k MOST INFLUENTIAL neighbors (panels CF).

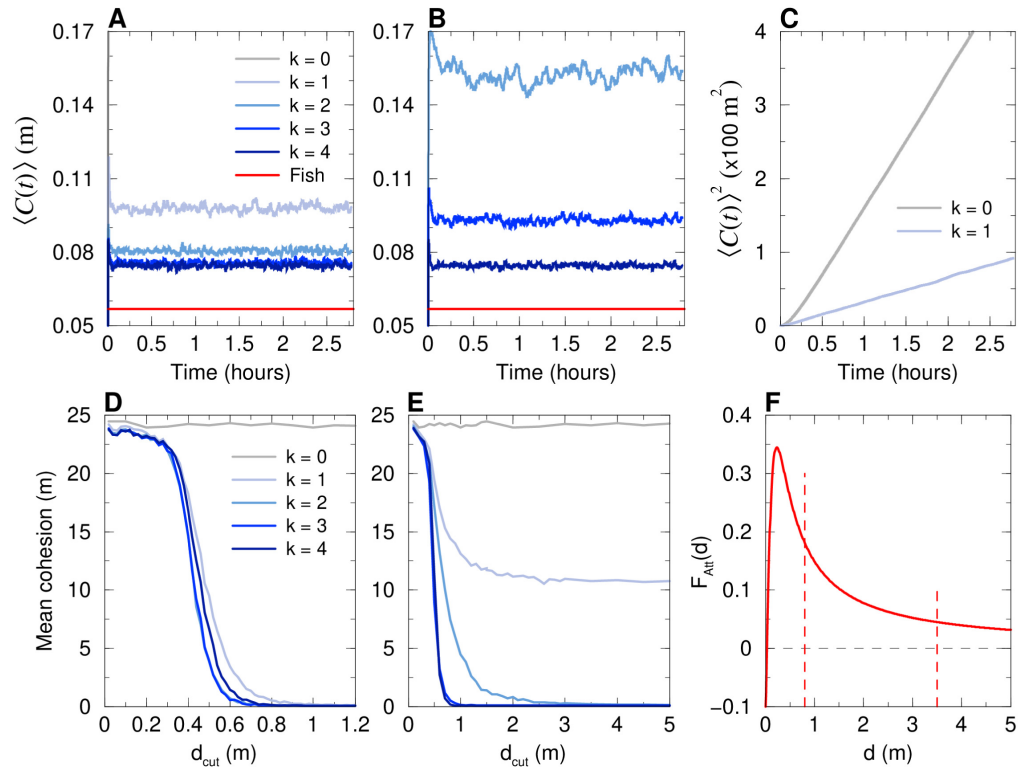


Fig 9. Average cohesion of a group of 5 agents swimming in an unbounded domain. Model simulations for the MOST INFLUENTIAL strategy (AD) and the NEAREST strategy (BCE), for $k = 1, \dots, 4$ (blue lines), together with the case with no interaction ($k = 0$, gray lines) and the mean cohesion for fish experiments (red lines in AB). For $k = 0$, cohesion is lost immediately, so that the gray line is not visible on the scale of panels AB. (C): Squared mean cohesion in the diffusive cases for $k = 1$ nearest neighbor and $k = 0$. (ABC): Average over 1000 runs with 10000 kicks (≈ 2.7 hours) per run. (DE): Mean cohesion averaged over the last 10% of the 1000 runs for different values of the cut-off distance d_{cut} for the two strategies: (D) MOST INFLUENTIAL, and (E) NEAREST. Panel (F): We plot the attraction function F_{Att} (see Eq. 10), showing the critical values d_{cut}^* above which cohesion is preserved (vertical dashed lines): $d_{\text{cut}}^* \sim 0.8$ m when the interacting neighbors are the $k = 1, 2$ or 3 most influential ones, the $k = 3$ nearest ones, or all the neighbors ($k = 4$); $d_{\text{cut}}^* \approx 3.5$ m when interacting with the $k = 2$ nearest neighbors (d_{cut}^* does not exist when interacting only with the nearest neighbor).

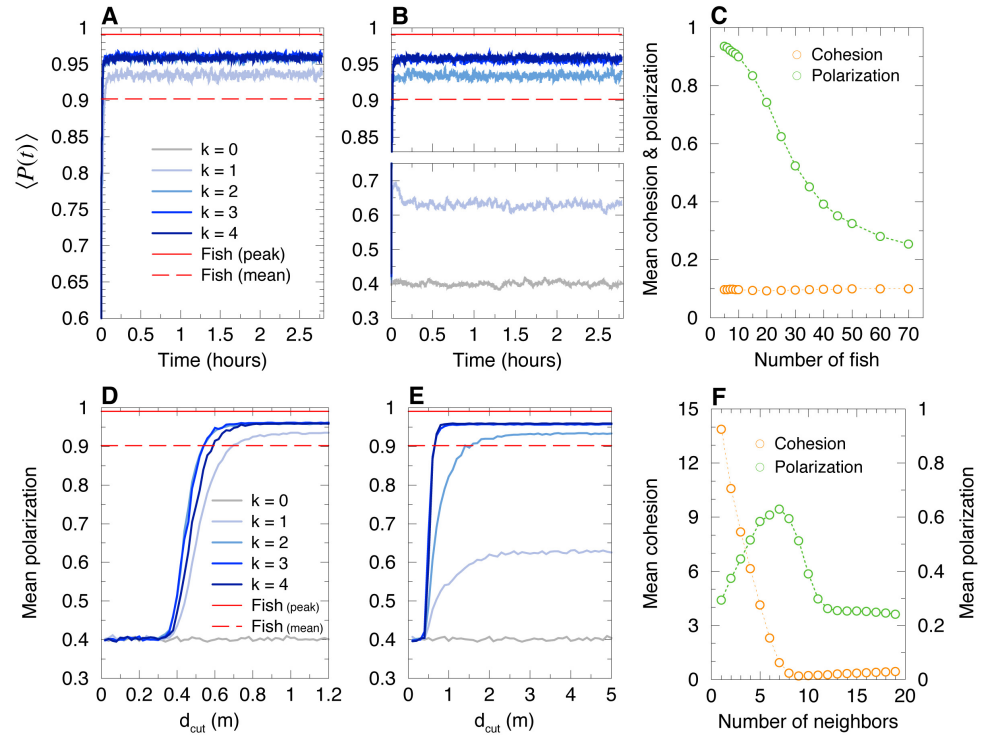


Fig 10. Average polarization of groups of 5 agents, and mean cohesion and polarization in larger groups ($N = 5, \dots, 70$), when agents are swimming in an unbounded domain. For $N = 5$, model simulations for the MOST INFLUENTIAL strategy (AD) and the NEAREST strategy (BE), for $k = 1, \dots, 4$ (blue lines), together with the case with no interaction ($k = 0$, gray lines) and the mean polarization for fish experiments (red lines). Panel (C): Mean cohesion and polarization in large groups ($N = 5, \dots, 70$) for the MOST INFLUENTIAL strategy ($k = 1$). Panel (F): Mean cohesion and polarization in a group of size $N = 20$ as a function of the number k of nearest neighbors with which focal individuals interact. The minimum of the cohesion is reached at $k = 9$, and the maximum of the polarization at $k = 7$.

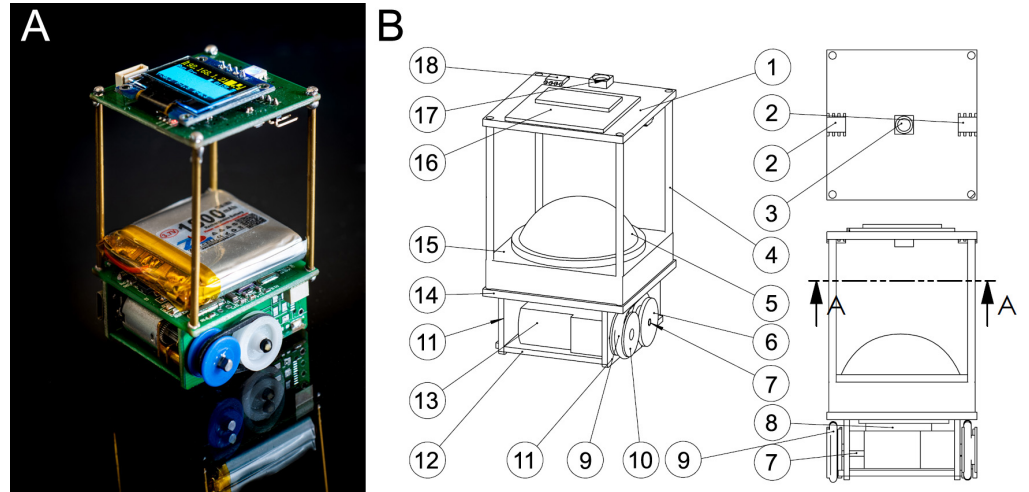


Fig 11. Cuboid robots. (A) Photograph of a Cuboid robot. Credits to David Villa ScienceImage/CBI/CNRS, Toulouse, 2018. (B) Design structure of Cuboid robot; A-A represents a cutaway view.

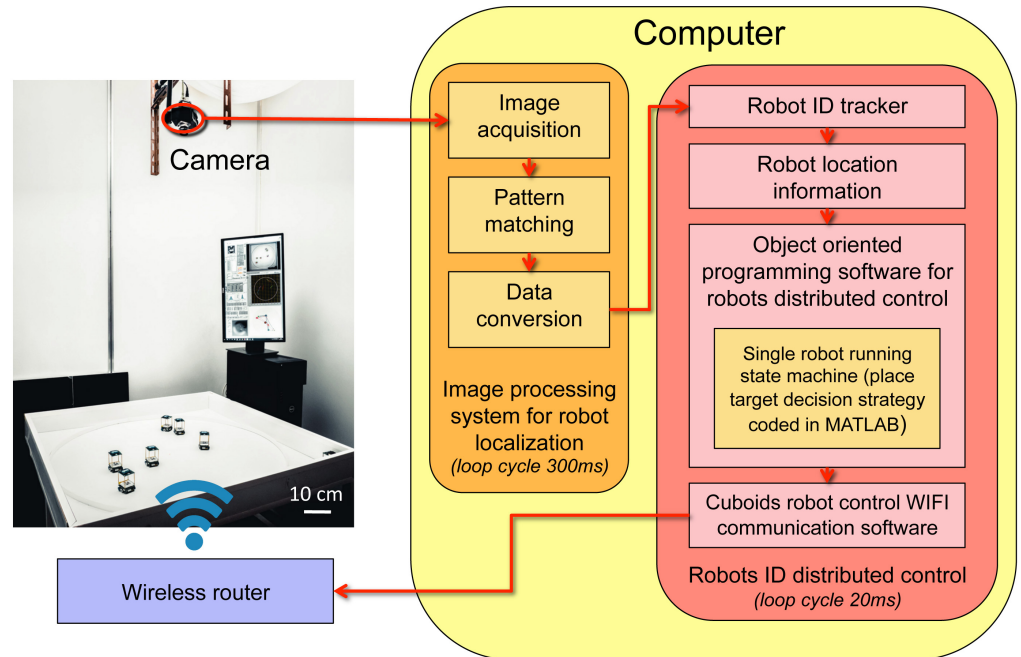


Fig 12. Structure of Cuboids platform. Two main parts: the physical hardware and the control software. The hardware consists of a square platform. A camera mounted on the top of it monitors the movements of Cuboids robots, which are controlled in a distributed way by a wireless router. The software processes the image acquired by the camera, then computes the command of actions to be performed by each robot, and finally sends the control signals to the robots via the WIFI channel. Then, all the robots execute their commands at the same time to perform the collective motion. The WIFI broadcasting is one-way communication for sending the command to the robots every 20 ms. In this setup, no information acquired by robots sensors is sent back to the computer though the WIFI channel. Credits to David Villa ScienceImage/CBI/CNRS, Toulouse, 2018.

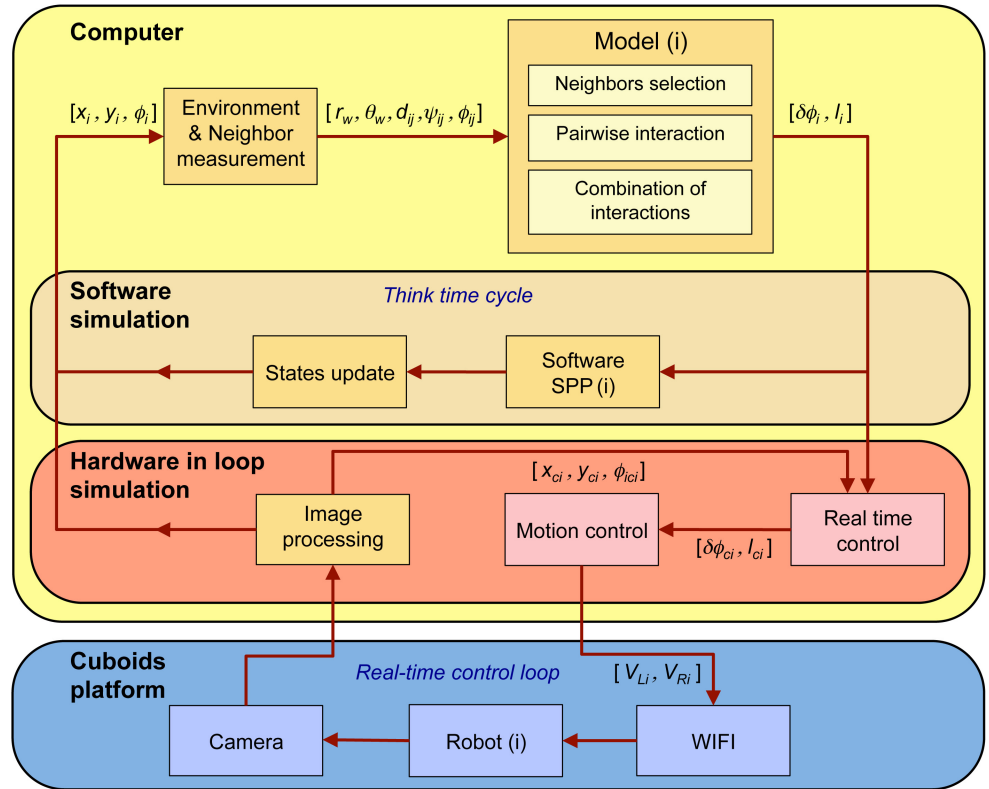


Fig 13. Software simulation and Hardware in Loop (HIL) simulation (from [42]). The structure of HIL is an extension of the software simulation, which consists of two extra parts: 1) a computer software (Image Processing, Motion Control, and Real Time Control modules) and 2) a physical hardware (Robot, camera and wireless router). In the software simulation, the Environment & Neighbor Measurement module converts the global position of a robot or a particle (x_i, y_i, ϕ_i) in the SPP software into local information ($r_{w,i}, \theta_{w,i}$) and ($d_{ij}, \psi_{ij}, \phi_{ij}$). Then the computational model generates a new kick decision in the form of heading variation and kick length ($\delta\phi_i, l_i$). This new decision ($\delta\phi_i, l_i$) is then directly sent to the SPP(i) software. Once the state has been updated, a new global position is provided by the SPP(i) software (brown box) or the Hardware in loop simulation (red box). By contrast, the HIL simulation includes hardware, *i.e.*, robots, camera and WIFI router (blue box). Furthermore, each robot i is controlled in real time by three more software modules running in the computer, which are the *Image Processing*, *Motion Control*, and *Real Time Control* modules (red box). The Image Processing module computes the global position of each robot ($x_{c,i}, y_{c,i}, \phi_{c,i}$) from the information provided by the camera in real time. Then, the Real Time Control module converts the model decision ($\delta\phi_i, l_i$) into a real time decision in the robot ($\delta\phi_{c,i}, l_{c,i}$), which are the heading variation and kick length to perform the decision based on its real time position ($x_{c,i}, y_{c,i}, \phi_{c,i}$). Finally, the Motion Control software generates left and right wheel motors speed control ($V_{L,i}, V_{R,i}$) for each robot to achieve its decision ($\delta\phi_{c,i}, l_{c,i}$). Each robot receives these motor commands by WIFI signals, and performs the corresponding movements that are monitored by the camera.

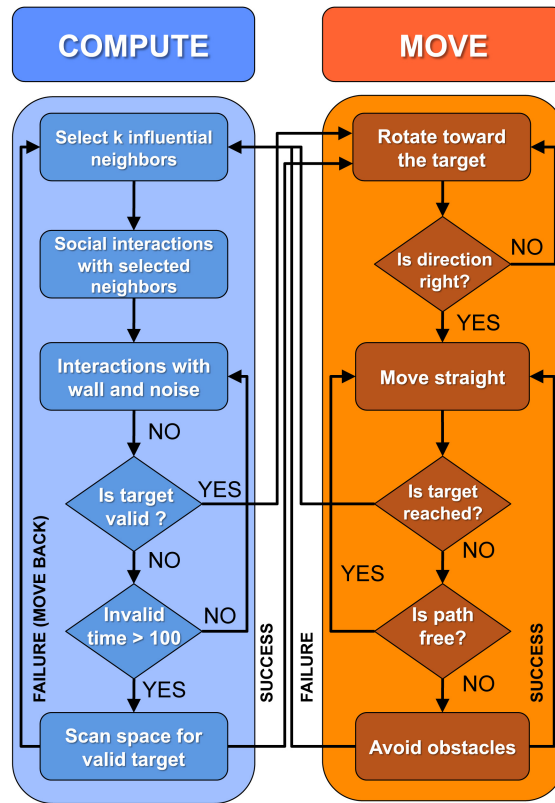


Fig 14. Flow chart of robot states machine. At any time a robot can be in one of the two following states: (1) the COMPUTE state for choosing a new target place, and (2) the MOVE state to reach the target place. In the COMPUTE state, the robot first selects influential neighbors, then it computes the pairwise influence of each neighbor, and finally it adds all influences to generate a new target place. Then, this new target place is validated to avoid collisions with the wall or another robot. If a valid target place cannot be found, the robot scans all space around itself for a valid target place. If the scanning method cannot find a valid target, the robot moves back over a distance of 80 mm and starts again the COMPUTE state. When a valid target place has been found, the robot switches into the MOVE state. The robot first rotates toward the target and then, moves straight to it. If another running neighbor blocks the path, the robot uses a procedure to avoid the obstacles.

| STRATEGY | | C | P | r_w^B | θ_w^B | Q | $\langle \text{All} \rangle$ |
|--------------------------|---------|-------|-------|---------|--------------|-------|------------------------------|
| | $k = 0$ | 0.909 | 0.532 | 0.341 | 0.145 | 0.023 | 0.390 |
| NEAREST | $k = 1$ | 0.369 | 0.178 | 0.034 | 0.041 | 0.003 | 0.125 |
| | $k = 2$ | 0.065 | 0.049 | 0.032 | 0.033 | 0.020 | 0.040 |
| | $k = 3$ | 0.013 | 0.026 | 0.027 | 0.032 | 0.037 | 0.027 |
| RANDOM | $k = 1$ | 0.310 | 0.223 | 0.095 | 0.068 | 0.009 | 0.141 |
| | $k = 2$ | 0.061 | 0.103 | 0.037 | 0.059 | 0.037 | 0.059 |
| | $k = 3$ | 0.012 | 0.062 | 0.028 | 0.048 | 0.038 | 0.038 |
| MOST INFLU- ENTIAL | $k = 1$ | 0.078 | 0.150 | 0.067 | 0.048 | 0.006 | 0.070 |
| | $k = 2$ | 0.011 | 0.051 | 0.025 | 0.080 | 0.033 | 0.040 |
| | $k = 3$ | 0.016 | 0.038 | 0.027 | 0.042 | 0.036 | 0.032 |
| | $k = 4$ | 0.014 | 0.042 | 0.024 | 0.044 | 0.030 | 0.031 |

Table 1. Model simulations vs fish experiments. Distance $D(\text{Fish} | \text{Model})$ between the probability distribution function (PDF) of the 5 observables used to quantify the collective motion in the fish model and the corresponding PDF obtained in fish experiments. We list the results for the 3 different interaction strategies implemented in the fish model and the associated value of k for the number of interacting neighbors. The last column $\langle \text{All} \rangle$ corresponds to the average of the 5 corresponding distances, an arbitrary but reasonable global quantifier to assess the overall agreement of a given condition with the results of fish experiments. For $k = 1$, the MOST INFLUENTIAL strategy gives significantly better results than the two other strategies and already leads to a fair agreement with fish experiments.

| STRATEGY | | C | P | r_w^B | θ_w^B | Q | $\langle \text{All} \rangle$ |
|---------------------|---------|-------|-------|---------|--------------|-------|------------------------------|
| | $k = 0$ | 0.604 | 0.561 | 0.238 | 0.114 | 0.170 | 0.337 |
| NEAREST | $k = 1$ | 0.418 | 0.486 | 0.158 | 0.070 | 0.239 | 0.274 |
| | $k = 2$ | 0.111 | 0.249 | 0.063 | 0.042 | 0.093 | 0.112 |
| | $k = 3$ | 0.066 | 0.039 | 0.083 | 0.036 | 0.026 | 0.05 |
| RANDOM | $k = 1$ | 0.140 | 0.343 | 0.040 | 0.107 | 0.065 | 0.139 |
| | $k = 2$ | 0.019 | 0.141 | 0.035 | 0.080 | 0.029 | 0.061 |
| | $k = 3$ | 0.056 | 0.063 | 0.095 | 0.042 | 0.025 | 0.056 |
| MOST INFLUENTIAL | $k = 1$ | 0.045 | 0.089 | 0.050 | 0.042 | 0.011 | 0.047 |
| | $k = 2$ | 0.028 | 0.050 | 0.031 | 0.088 | 0.024 | 0.044 |
| | $k = 4$ | 0.078 | 0.080 | 0.040 | 0.053 | 0.038 | 0.058 |

Table 2. Collective robotics experiments vs fish experiments. Distance $D(\text{Fish} | \text{Robots})$ between the probability distribution function (PDF) of the 5 observables used to quantify the collective motion of the robots and the corresponding PDF obtained in fish experiments. We list the results for the 3 different interaction strategies implemented in the fish model and the associated value of k for the number of interacting neighbors. The last column $\langle \text{All} \rangle$ corresponds to the average of the 5 corresponding distances, an arbitrary but reasonable global quantifier to assess the overall agreement of a given condition with the results of fish experiments. For $k = 1$, the MOST INFLUENTIAL strategy gives significantly better results than the two other strategies and already leads to a fair agreement with fish experiments.

| Parameter | Symbol | Model | Robots |
|-----------------------------------------------------|----------------|-------|--------|
| Intensity of heading random fluctuations | γ_R | 0.45 | 0.1 |
| Fluctuations reduction factor when close to wall | α | 0.67 | 1 |
| Intensity of wall repulsion | γ_w | 0.15 | 0.79 |
| Range of wall repulsion (cm) | l_w | 6 | 11 |
| Intensity of attraction/repulsion | γ_{Att} | 0.12 | 0.18 |
| Range of attraction between individuals (cm) | l_{Att} | 20 | 37 |
| Distance of balance of attraction/repulsion (cm) | d_{Att} | 3 | 18 |
| Intensity of alignment | γ_{Ali} | 0.09 | 0.04 |
| Range of alignment between individuals (cm) | l_{Ali} | 20 | 37 |
| Distance of alignment (cm) | d_{Ali} | 6 | 5 |
| Average duration between successive kicks (s) | τ | 0.5 | 1.3 |
| Mean length between two successive kicks (cm) | l | 7 | 7.4 |
| Typical individual velocity in active period (cm/s) | v_0 | 14 | 3.75 |
| Relaxation time (s) | τ_0 | 0.8 | 0.9 |

Table 3. Values and units of the parameters for model simulations and robot experiments.

1372 **Supporting Information**

1373 **Supporting figures**

1374 **S1 Fig. Density maps of the polarization vs cohesion for fish and model**
 1375 **simulations, normalized with the total number of data.**

1376 Density maps are shown for fish experiments (FISH panel) and for the 11 strategies
 1377 considered in the model simulations. The color intensity corresponds to the number of
 1378 data in each box normalized with the total number of data in the grid ($\times 1000$). We
 1379 used 40×50 boxes.

1380 **S2 Fig. Density maps of polarization vs cohesion for fish and model simu-**
 1381 **lations, normalized with the number of data per range of polarization.**

1382 Density maps are shown for fish experiments (FISH panel) and for the 11 strategies
 1383 considered in the model simulations. The color intensity corresponds to the number of
 1384 data in each box normalized with the number of data per interval of polarization, *i.e.*,
 1385 each row is the PDF of the cohesion for a range of values of the polarization. We used
 1386 40×50 boxes.

1387 **S3 Fig. Density maps of polarization vs cohesion for fish and robot groups,**
 1388 **normalized with the total number of data.**

1389 Density maps are shown for fish experiments (FISH panel) and for the 10 strategies
 1390 considered in the robot experiments. The color intensity corresponds to the number of
 1391 data in each box normalized with the total number of data in the grid ($\times 1000$). We
 1392 used 40×50 boxes.

1393 **S4 Fig. Density maps of polarization vs cohesion for fish and robot groups,**
 1394 **normalized with the number of data per range of polarization.**

1395 Density maps are shown for fish experiments (FISH panel) and for the 10 strategies
 1396 considered in the robot experiments. The color intensity corresponds to the number of
 1397 data in each box normalized with the number of data per interval of polarization, *i.e.*,
 1398 each row is the PDF of the cohesion for a range of values of the polarization. We used
 1399 40×50 boxes.

1400 **S5 Fig. Counter-milling in model simulations.** Red arrows represent the velocity
 1401 field of agents in the reference system of the barycenter of the group, here located at
 1402 coordinates $(0, 0)$. Orange circle denotes the average relative position of the border of
 1403 the arena with respect to the barycenter. The cases where agents interact with the $k = 3$
 1404 most influential neighbors (statistically identical to the case where $k = 4$) and where
 1405 agents do not interact ($k = 0$) are not shown.

1406 **S6 Fig. Counter-milling in robotic experiments.** Red arrows represent the
 1407 velocity field of robots in the reference system of the barycenter of the group, here
 1408 located at coordinates $(0, 0)$. Orange circle denotes the average relative position of the
 1409 border of the arena with respect to the barycenter. The cases where robots interact with
 1410 the $k = 3$ most influential neighbors (statistically identical to the case where $k = 4$) and
 1411 where robots do not interact ($k = 0$) are not shown.

1412 **S7 Fig. Average cohesion and polarization for group sizes $N = 5, \dots, 20$**
 1413 **(N even) when each individual interacts with its k nearest neighbors, for**
 1414 **$k = 1, \dots, N - 1$.** Mean cohesion (A) and mean polarization (B) as a function of k .
 1415 Cohesion values are scaled with $\lambda_M = 0.87$. In panel (A), high values of the cohesion for
 1416 small values of k with respect to the group size N are not shown (vertical lines grow up
 1417 to 20 m in our simulations as the individuals diffuse independently of each other). In
 1418 (B), the values of k for $N = 22, 24$ and 26 (marked with an asterisk in the legend) are
 1419 limited to the interval of interest [8, 12].

1420 **S8 Fig. Finite state machine diagram of one robot.** The decision-making
 1421 processes of the robot (COMPUTE state) are shown in blue. The movements of the
 1422 robot (MOVE state) are shown in brown. In the COMPUTE state, the model determines
 1423 a new target to reach by integrating the local information about the neighbors and the
 1424 environment. A target is valid when this one is not blocked by the wall or other robots.
 1425 If the target is invalid, the computer tries to find a new target by the scanning method.
 1426 If the scanning fails, the robot moves back 80 mm and starts again for model computing.
 1427 If the decision target is valid, the robot switches into MOVE state, which includes three
 1428 sub-states: Rotate, Move straight, and Avoid obstacle. The robot first rotates towards
 1429 to the target and then moves straight to it. If a running neighbor blocks the path, the
 1430 robot uses a procedure to avoid the obstacle.

1431 **S9 Fig. Interaction functions with the wall and between individuals, ex-**
 1432 **tracted from experiments of fish swimming in pairs [14].** (A) Intensity of the
 1433 repulsion from the wall $F_w(r_{w,i})$ (green) as a function of the distance to the wall $r_{w,i}$,
 1434 and intensity of the attraction $F_{Att}(d_{ij})$ (red) and the alignment $F_{Ali}(d_{ij})$ (blue) between
 1435 fish i and j as functions of the distance d_{ij} separating them. (B) Normalized odd angular
 1436 function $O_w(\theta_{w,i})$ modulating the interaction with the wall as a function of the relative
 1437 angle to the wall $\theta_{w,i}$. (C) Normalized angular functions $O_{Att}(\psi_{ij})$ (odd, in red) and
 1438 $E_{Att}(\phi_{ij})$ (even, in orange) of the attraction interaction, and (D) $O_{Ali}(\phi_{ij})$ (odd, in blue)
 1439 and $E_{Ali}(\psi_{ij})$ (even, in violet) of the alignment interaction between agents i and j , as
 1440 functions of the angle of perception ψ_{ij} and the relative heading ϕ_{ij} .

1441 Supporting videos

1442 **S1 Video. Collective movements in rummy-nose tetra (*Hemigrammus rhodos-***
 1443 ***tomus*).** A typical experiment with a group of 5 fish swimming in a circular tank of
 1444 radius 250 mm.

1445 **S2 Video. Collective motion in a group of 5 robots.** Each robot interacts with
 1446 its most influential neighbor. The video is accelerated 9 times. Total duration: 7.15
 1447 minutes.

1448 **S3 Video. Tracking and analysis output.** The small circles superimposed on
 1449 the trajectories represents the kicks performed by the fish when the speed reaches its
 1450 maximum value.

1451 **S4 Video. Counter milling behavior in a group of 5 fish.** Top: Typical experi-
 1452 ment with a group of 5 fish in a circular arena of radius 250 mm. The video is accelerated
 1453 6 times. Total duration 1.3 minutes. Bottom: Relative movement of fish with respect to
 1454 the barycenter of the group, represented by the black arrow on top video and a black
 1455 disk on the bottom video. Fish turn counter-clockwise around the tank and clockwise
 1456 with respect to the barycenter.

1457 **S5 Video. Collective robotics experiment without any social interaction**
 1458 **between the robots ($k = 0$) and only obstacle avoidance behavior is at play.**
 1459 Top: Typical experiment with a group of 5 robots in a circular arena of radius 420 mm,
 1460 captured by the top camera. The border of the arena is represented by the red circle.
 1461 Purple circles represent the individual robot safety area, of diameter 8 cm. Small green
 1462 dots in front of robots indicate their next target place. The video is accelerated 6 times.
 1463 Total duration: 6 minutes. Bottom: Relative movement of the robots with respect to the
 1464 barycenter of the group. The barycenter is represented by the black disk and remains
 1465 oriented to the right. Robots are represented by colored disks with their identification
 1466 number in the center. The small circle at the front of a robot indicates its heading. The
 1467 arrows represent the interactions between robots. Arrow direction indicates the identity
 1468 (color) of the robot that exerts its influence on the robot to which the arrow points. The
 1469 small dots in front of the robots represent the next target places.

1470 **S6 Video. Collective robotics experiment where robots interact with the**
 1471 **$k = 1$ nearest neighbor.** Top: Typical experiment with a group of 5 robots in a
 1472 circular arena of radius 420 mm, captured by the top camera. The border of the arena is
 1473 represented by the red circle. Purple circles represent the individual robot safety area, of
 1474 diameter 8 cm. Small green dots in front of robots indicate their next target place. The
 1475 video is accelerated 6 times. Total duration: 6 minutes. Bottom: Relative movement of
 1476 the robots with respect to the barycenter of the group. The barycenter is represented
 1477 by the black disk and remains oriented to the right. Robots are represented by colored
 1478 disks with their identification number in the center. The small circle at the front of
 1479 a robot indicates its heading. The arrows represent the interactions between robots.
 1480 Arrow direction indicates the identity (color) of the robot that exerts its influence on
 1481 the robot to which the arrow points. The small dots in front of the robots represent the
 1482 next target places.

1483 **S7 Video. Collective robotics experiment where robots interact with the**
 1484 **$k = 1$ most influential neighbor.** Top: Typical experiment with a group of 5 robots
 1485 in a circular arena of radius 420 mm, captured by the top camera. The border of the
 1486 arena is represented by the red circle. Purple circles represent the individual robot safety
 1487 area, of diameter 8 cm. Small green dots in front of robots indicate their next target
 1488 place. The video is accelerated 6 times. Total duration: 6 minutes. Bottom: Relative
 1489 movement of the robots with respect to the barycenter of the group. The barycenter is
 1490 represented by the black disk and remains oriented to the right. Robots are represented
 1491 by colored disks with their identification number in the center. The small circle at the
 1492 front of a robot indicates its heading. The arrows represent the interactions between
 1493 robots. Arrow direction indicates the identity (color) of the robot that exerts its influence
 1494 on the robot to which the arrow points. The small dots in front of the robots represent
 1495 the next target places.

1496 **S8 Video. Collective robotics experiment where robots interact with $k = 1$**
 1497 **randomly selected neighbor.** Top: Typical experiment with a group of 5 robots in a
 1498 circular arena of radius 420 mm, captured by the top camera. The border of the arena is
 1499 represented by the red circle. Purple circles represent the individual robot safety area, of
 1500 diameter 8 cm. Small green dots in front of robots indicate their next target place. The
 1501 video is accelerated 6 times. Total duration: 6 minutes. Bottom: Relative movement of
 1502 the robots with respect to the barycenter of the group. The barycenter is represented
 1503 by the black disk and remains oriented to the right. Robots are represented by colored
 1504 disks with their identification number in the center. The small circle at the front of
 1505 a robot indicates its heading. The arrows represent the interactions between robots.
 1506 Arrow direction indicates the identity (color) of the robot that exerts its influence on
 1507 the robot to which the arrow points. The small dots in front of the robots represent the
 1508 next target places.

1509 **S9 Video. Collective robotics experiment where robots interact with the**
 1510 **$k = 2$ nearest neighbors.** Top: Typical experiment with a group of 5 robots in a
 1511 circular arena of radius 420 mm, captured by the top camera. The border of the arena is
 1512 represented by the red circle. Purple circles represent the individual robot safety area, of
 1513 diameter 8 cm. Small green dots in front of robots indicate their next target place. The
 1514 video is accelerated 6 times. Total duration: 6 minutes. Bottom: Relative movement of
 1515 the robots with respect to the barycenter of the group. The barycenter is represented
 1516 by the black disk and remains oriented to the right. Robots are represented by colored
 1517 disks with their identification number in the center. The small circle at the front of
 1518 a robot indicates its heading. The arrows represent the interactions between robots.
 1519 Arrow direction indicates the identity (color) of the robot that exerts its influence on
 1520 the robot to which the arrow points. The small dots in front of the robots represent the
 1521 next target places.

1522 **S10 Video. Collective robotics experiment where robots interact with the**
 1523 **$k = 2$ most influential neighbors.** Top: Typical experiment with a group of 5 robots
 1524 in a circular arena of radius 420 mm, captured by the top camera. The border of the
 1525 arena is represented by the red circle. Purple circles represent the individual robot safety
 1526 area, of diameter 8 cm. Small green dots in front of robots indicate their next target
 1527 place. The video is accelerated 6 times. Total duration: 6 minutes. Bottom: Relative
 1528 movement of the robots with respect to the barycenter of the group. The barycenter is
 1529 represented by the black disk and remains oriented to the right. Robots are represented
 1530 by colored disks with their identification number in the center. The small circle at the
 1531 front of a robot indicates its heading. The arrows represent the interactions between
 1532 robots. Arrow direction indicates the identity (color) of the robot that exerts its influence
 1533 on the robot to which the arrow points. The small dots in front of the robots represent
 1534 the next target places.

1535 **S11 Video. Collective robotics experiment where robots interact with $k = 2$**
 1536 **randomly selected neighbors.** Top: Typical experiment with a group of 5 robots in
 1537 a circular arena of radius 420 mm, captured by the top camera. The border of the arena
 1538 is represented by the red circle. Purple circles represent the individual robot safety area,
 1539 of diameter 8 cm. Small green dots in front of robots indicate their next target place.
 1540 The video is accelerated 6 times. Total duration: 6 minutes. Bottom: Relative movement
 1541 of the robots with respect to the barycenter of the group. The barycenter is represented

1542 by the black disk and remains oriented to the right. Robots are represented by colored
 1543 disks with their identification number in the center. The small circle at the front of
 1544 a robot indicates its heading. The arrows represent the interactions between robots.
 1545 Arrow direction indicates the identity (color) of the robot that exerts its influence on
 1546 the robot to which the arrow points. The small dots in front of the robots represent the
 1547 next target places.

1548 **S12 Video. Collective robotics experiment where robots interact with the**
 1549 **$k = 3$ nearest neighbors.** Top: Typical experiment with a group of 5 robots in a
 1550 circular arena of radius 420 mm, captured by the top camera. The border of the arena is
 1551 represented by the red circle. Purple circles represent the individual robot safety area, of
 1552 diameter 8 cm. Small green dots in front of robots indicate their next target place. The
 1553 video is accelerated 6 times. Total duration: 6 minutes. Bottom: Relative movement of
 1554 the robots with respect to the barycenter of the group. The barycenter is represented
 1555 by the black disk and remains oriented to the right. Robots are represented by colored
 1556 disks with their identification number in the center. The small circle at the front of
 1557 a robot indicates its heading. The arrows represent the interactions between robots.
 1558 Arrow direction indicates the identity (color) of the robot that exerts its influence on
 1559 the robot to which the arrow points. The small dots in front of the robots represent the
 1560 next target places.

1561 **S13 Video. Collective robotics experiment where robots interact with $k = 3$**
 1562 **randomly selected neighbors.** Top: Typical experiment with a group of 5 robots in
 1563 a circular arena of radius 420 mm, captured by the top camera. The border of the arena
 1564 is represented by the red circle. Purple circles represent the individual robot safety area,
 1565 of diameter 8 cm. Small green dots in front of robots indicate their next target place.
 1566 The video is accelerated 6 times. Total duration: 6 minutes. Bottom: Relative movement
 1567 of the robots with respect to the barycenter of the group. The barycenter is represented
 1568 by the black disk and remains oriented to the right. Robots are represented by colored
 1569 disks with their identification number in the center. The small circle at the front of
 1570 a robot indicates its heading. The arrows represent the interactions between robots.
 1571 Arrow direction indicates the identity (color) of the robot that exerts its influence on
 1572 the robot to which the arrow points. The small dots in front of the robots represent the
 1573 next target places.

1574 **S14 Video. Collective robotics experiment where robots interact with all**
 1575 **their neighbors ($k = 4$).** Top: Typical experiment with a group of 5 robots in a
 1576 circular arena of radius 420 mm, captured by the top camera. The border of the arena is
 1577 represented by the red circle. Purple circles represent the individual robot safety area, of
 1578 diameter 8 cm. Small green dots in front of robots indicate their next target place. The
 1579 video is accelerated 6 times. Total duration: 6 minutes. Bottom: Relative movement of
 1580 the robots with respect to the barycenter of the group. The barycenter is represented
 1581 by the black disk and remains oriented to the right. Robots are represented by colored
 1582 disks with their identification number in the center. The small circle at the front of
 1583 a robot indicates its heading. The arrows represent the interactions between robots.
 1584 Arrow direction indicates the identity (color) of the robot that exerts its influence on
 1585 the robot to which the arrow points. The small dots in front of the robots represent the
 1586 next target places.